4. 2644

ORNL-5510

Irradiation Performance of HTGR Fuel in HFIR Capsule HT-31

T. N. Tiegs
J M Robbins
R. L. Hamner
B. H. Montgomery
M. J. Kania
T. B. Lindemer
C. S. Morgan

ORNL-5510
Distribution
Category UC-77

Contract No W-7405-eng-26

METALS AND CERAMICS DIVISION

HTGR BASE TECHNOLOGY PROGRAM

Fueled Graphite Development (189a 01330)

IRRADIATION PERFORMANCE OF HTGR FUEL IN HFIR CAPSULE HT-31

T. N. Tiegs, J M Robbins, R. L. Hamner, B. H. Montgomery,
M. J. Kania, T. B. Lindemer, and C. S. Morgan

Date Published: May 1979

OAK RIDGE NATIONAL LABORATORY
Oak Ridge, Tennessee 37830
operated by
UNION CARBIDE CORPORATION
for the
DEPARTMENT OF ENERGY

CONTENTS

IRRADIATION PERFORMANCE OF HTGR FUEL IN HFIR CAPSULE HT-31

T. N. Tiegs, J M Robbins, R. L. Hamner, B. H. Montgomery,*
M. J. Kania, T. B. Lindemer,† and C. S. Morgan

ABSTRACT

Irradiation capsule HT-31 was a cooperative effort between General Atomic Company, Los Alamos Scientific Laboratory, and Oak Ridge National Laboratory (ORNL). The present report describes the ORNL portion of the experiment only.

The capsule was irradiated in the High Flux Isotope Reactor at ORNL to peak particle temperatures up to 1600°C, fast neutron fluences (0.18 MeV) up to 9×10^{25} n/m^2, and burnups up to 8.9% FIMA for ThO_2 particles.

The oxygen release from plutonium fissions was less than calculated, possibly because of the solid solution of SrO and rare earth oxides in UO_2.

Tentative results show that pyrocarbon permeability decreases with increasing fast neutron fluence.

Fission products in sol-gel UO_2 particles containing natural uranium mostly behaved similarly to those in particles containing highly enriched uranium (HEU). Thus, much of the data base collected on HEU fuel can be applied to low-enriched fuel. Fission product palladium penetrated into the SiC on Triso-coated particles. Also the SiC coating provided some retention of ^{110m}Ag.

Irradiation above about 1200°C without an outer pyrocarbon coating degraded the SiC coating on Triso-coated particles.

1. INTRODUCTION

Irradiation capsule HT-31 was a cooperative effort between General Atomic Company (GA), Los Alamos Scientific Laboratory (LASL), and Oak Ridge National Laboratory (ORNL). This report will describe the ORNL portion of the experiment only, while the GA and LASL portions of the experiment will be reported by them.[1,2]

The capsule was designed as a four-cycle experiment in High Flux Isotope Reactor (HFIR) operating at graphite sleeve temperatures of 950 and 1250°C. The top half of the capsule contained loose coated inert particles from ORNL and bonded rods from LASL and ORNL. The lower half

*Engineering Technology Division.
†Chemical Technology Divison.

contained loose coated fertile ThO_2 particles from GA and particles from ORNL containing low-enriched uranium and designed for heat generation.

The ORNL objectives were as follows:

1. The primary objective of the ORNL bonded rods was to furnish supplemental data to replace that information lost when certain specimens from previous experiments (HT-20, -21, -22, and -23) were broken during disassembly. The purpose of these rods was to provide measurements of changes in thermal conductivity, electrical resistivity, thermal expansion, and dimensions as functions of particle volume loading and fast neutron fluence.

2. A secondary objective of the experiment involved furnishing coated $^{238}UO_2$ particles to more accurately determine the internal gas pressure of irradiated particles. This information is important to the design of HTGR fuel particles. Normal UO_2 particles were used instead of $^{235}UO_2$ particles because a larger supply could be irradiated in an HT capsule, and any enrichment above about 7% would result in excessive power production early in the irradiation and cause very high temperatures.

3. A peripheral experiment involved the irradiation of a small graphite crucible containing carbon-coated inert particles to supply neutron damaged particles for coating permeability studies.

2. DESCRIPTION OF EXPERIMENT

The design of this capsule was identical to that[3] of capsule HT-28. A schematic of the capsule design is shown in Fig. 1. The loading scheme and heavy metal loadings are shown in Tables 1 and 2, respectively.

Crucible 1 contained loose coated inert particles for coating studies and 1.024 g Re as an additional gamma heat source to obtain the desired 950°C graphite sleeve temperature. The rhenium was in the form of foil disks distributed throughout the length of the crucible separated by layers of loose particles. The descriptions of these particles and pertinent fabrication data are presented in Tables 3, 4, and 5.

Bonded rod ORNL-1 was an unirradiated slug-injected annular rod containing about 58 vol % inert Biso-coated particles. The central hole

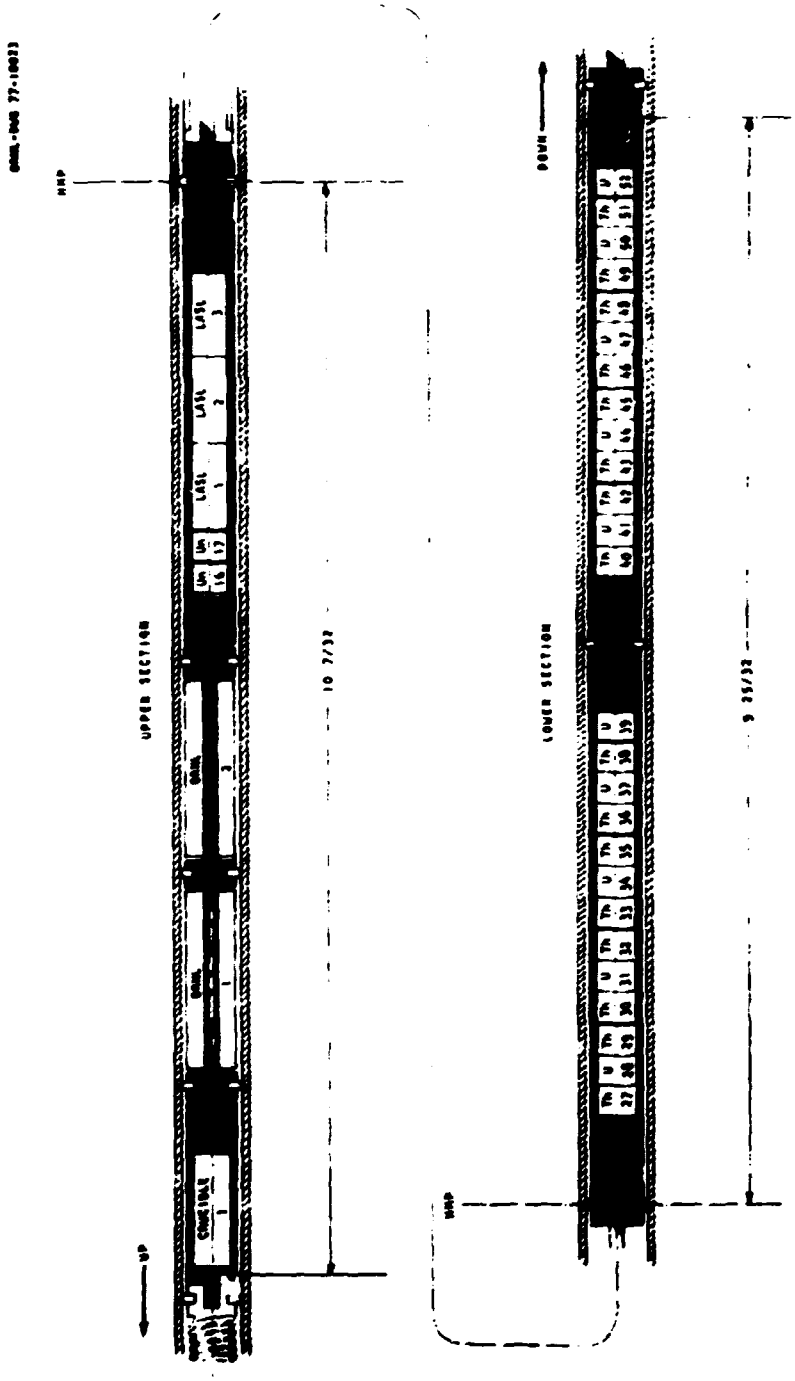

Fig. 1. Schematic Diagram of Sample Placement in HFIR Irradiation Capsules HT-31 and HT-32. Lengths shown are in inches. They correspond to 259.6 and 248.4 mm.

Table 1. Loading Scheme — Capsule HT-31

Position[a]	Type Specimen	Fuel (HM)[b]	Batch[c]	Type Coating
		Low-Temperature Zone - Upper Half		
Crucible 1	Loose particles	Carbon	OR-2294-HT	Biso
ORNL-1	Slug-injected rod; 58 vol % coated particles	Carbon	OR-2305-FH	Biso
ORNL-2	Extrusion; 35 vol % coated particles	Carbon	OR-2081-H	Biso
			OR-2084-H	Biso
			OR-2085-H	Biso
			OR-2086-H	Biso
		Magazine 16 - High-Temperature Zone - Upper Half		
16	Loose particles	Sol-gel UO_2	OR-2511-H	Biso
17	Loose particles	Sol-gel UO_2	OR-2533-H	Triso
LASL-1		Uranium	OR-2257-H	Triso
		Thorium	GA-6291 - composite 3	Biso
LASL-2	Extrusions	Carbon	LASL 76-53HT	Triso (ZrC)
LASL-3		Carbon	LASL 76-54HT	Triso (ZrC)
		Magazine 15 - High-Temperature Zone - Lower Half		
Top end plug	Loose particles	Uranium	OR-2248-H	Triso
27		Thorium	6252-05-0160-006	
28		Uranium	OR-2248-H[d]	
29		Thorium	6252-08-0161-002	
30		Thorium	6252-10-0161-002	
31		Uranium	OR-2248-H[d]	
32		Thorium	6252-09-0161-002	
33		Thorium	6252-07-0261-002	
34		Uranium	OR-2248-H[d]	
35		Thorium	6252-07-0161-002	
36		Thorium	6252-06-0261-002	
37		Uranium	OR-2248-H[d]	
38		Thorium	6252-06-0161-002	
39		Uranium	OR-2248-H[d]	
		Magazine 14 - Low-Temperature Zone - Lower Half		
Top end plug	Loose particles	Uranium	OR-2248-H	Triso
40		Thorium	6252-10-0161-001	
41		Uranium	OR-2248-H[d]	
42		Thorium	6252-09-0161-001	
43		Thorium	6252-05-0160-005	
44		Uranium	OR-2248-H[d]	
45		Thorium	6252-07-0261-001	
46		Thorium	6252-07-0161-001	
47		Uranium	OR-2248-H[d]	
48		Thorium	6252-06-0261-001	
49		Thorium	6252-06-0161-001	
50		Uranium	OR-2248-H[d]	
51		Thorium	6252-08-0161-001	
52		Uranium	OR-2248-H[d]	

[a] Refer to Fig. 1.

[b] All heavy metal is in combined form; the thorium is $^{232}ThO_2$ from GA.

[c] Kernel in OR-2257-H is (WAR) $UC_{5.91}O_{1.26}$; kernel in OR-2248-H is WAR $UC_{0.86}O_{1.22}$.

[d] Outer LTI burned off.

Table 2. Heavy Metal Loadings — Capsule HT-31

Position	Loading, g			Enrichment (at. %)	Number of Particles
	Uranium	^{235}U	Thorium		
Magazine 16 — High-Temperature Zone — Upper Half					
16	0.01	<0.0001		0.7	
17	0.01	<0.0001		0.7	
LASL-1	0.0192	<0.0012	0.0396	6.36	
LASL-2	0.0180	<0.0011	0.0587	6.36	
LASL-3	0.0187	<0.0012	0.0541	6.36	
Magazine 15 — High-Temperature Zone — Lower Half					
Top end plug	0.0223	0.0014		6.5	
27			0.0334		51
28	0.0223	0.0014		6.5	
29			0.0331		80
30			0.0333		79
31	0.0223	0.0014		6.5	
32			0.0332		78
33			0.0330		78
34	0.0223	0.0014		6.5	
35			0.0332		80
36			0.0326		77
37	0.0223	0.0014		6.5	
38			0.0334		78
39	0.0223	0.0014		6.5	
Magazine 14 — Low-Temperature Zone — Lower Half					
Top end plug	0.0159	0.0010		6.5	
40			0.0223		53
41	0.0159	0.0010		6.5	
42			0.0226		53
43			0.0222		34
44	0.0159	0.0010		6.5	
45			0.0224		53
46			0.0224		54
47	0.0159	0.0010		6.5	
48			0.0220		52
49			0.0227		53
50	0.0159			6.5	
51			0.0224		54
52	0.0159	0.0010		6.5	

Table 3. Compositional Characterization of Coated Particles for HT-31[a]

Batch	Kernel Material	Uranium Content (wt %)	^{235}U Enrichment (at. %)	Positions in Capsule
OR-2305-FH	SAR carbon[b]			ORNL-1
OR-2086-H	SAR carbon			ORNL-2
OR-2511-H	sol-gel UO_2	29.10	normal	17
OR-2533-H	sol-gel UO_2	25.17	normal	16
OR-2248-H[c]	$UC_{4.86}O_{1.22}$	21.31	6.53	28, 31, 34, 37, 39, 41, 44, 47, 50, 52
OR-2248-H	$UC_{4.86}O_{1.22}$	15.67	6.53	Top end plug magazines 14, 15
OR-2294-HT	SAR carbon			Crucible 1

[a]Coated at ORNL.

[b]Desulfurized strong-acid resin (SAR).

[c]With outer LTI burned off.

Table 4. Mean Dimensions and Densities[a] of Coated Particles for HT-31 Coated at ORNL[b]

Batch	Kernel Diameter (μm)	Thickness, μm				Density, g/cm³				
		Buffer	Inner C	SiC	Outer C	Kernel	Buffer	Inner C	SiC	Outer C
OR-2305-HN	324 (18.1)	92.3 (12.7)			114.3 (7.2)	1.428	1.20			2.14
OR-2086-H	471.5 (24.6)	74			83.3 (5.5)	1.37	0.94			1.958 (0.011)
OR-2511-H	308.8 (2.9)	182.7 (16.5)			96.6 (4.3)	10.65	1.19			2.037 (0.006)
OR-2533-H	398.9 (2.3)	196.3 (18.2)	46.9 (3.0)	41.8 (3.7)	42.4 (2.4)	10.65	1.19	2.045 (0.016)	3.203 (0.003)	2.107 (0.006)
OR-2248-H	422.6 (33.9)	55.1 (11.1)	40.7 (4.8)	38.9 (1.7)	burned off	2.87	1.12	1.934 (0.008)	3.184 (0.011)	
OR-2248-H	422.6 (33.9)	55.1 (11.1)	40.7 (4.8)	38.9 (1.7)	46.8 (3.3)	2.87	1.12	1.934 (0.008)	3.184 (0.011)	2.02 (0.005)
OR-2294-HT	459.8 (29.3)	81.4 (9.6)			86.9 (4.3)	1.33	1.13			

[a]Numbers in parentheses are standard deviations.

[b]All these particles were annealed at 1800°C for 10 min before insertion into the capsule.

Table 5. Conditions for Coating Particles for HT-31

Batch	Buffer Coating[a] Temperature (°C)	Deposition Rate, μm/min			
		Buffer	Inner LTI[b]	SiC[c]	Outer LTI[b]
OR-2305-FH	1250	5.77			8.16
OR-2086-H	1300	5.29			5.95
OR-2511-H	1125	21.24			32.50
OR-2533-H	1125	21.24	33.03	0.25	24.33
OR-2248-H	1125	9.18	6.26	0.26	9.85
OR-2294-H	1250	5.09			3.34

[a]Deposited from C_2H_2

[b]Deposited from MAPP gas at 1275°C.

[c]Deposited from CH_3SiCl_3 at 1550°C.

contained approximately 2.2 g W to provide gamma heat generation during irradiation. The rod was fabricated with 29 wt % Asbury 6353 graphite filler and 71 wt % Ashland A-240 pitch binder. It was injected at 185°C and 6.20 MPa (900 psi) and carbonized in packed natural flake graphite. Extruded annular rod ORNL-2 contained about 35 vol % inert Biso-coated particles that had been irradiated in experiment HT-23 for two cycles.[4] It was fabricated with 58.7 wt % GLC*-1008 graphite powder (–60 mesh), 18.8 wt % raw Thermax† carbon black, 21.7 wt % Varcum‡ binder, and 0.8 wt % maleic anhydride (used as a catalyst). The rod was extruded at room temperature and 6.89 MPa (1000 psi). It was cured at 90°C for 16 h, carbonized at 1000°C, and heat-treated at 1800°C for 0.5 h. Properties of ORNL-1 and -2 are given in Table 6. Details on the particles used in the rods are presented in Tables 3, 4, and 5.

Small graphite holders designated U-16 and U-17 contained 10 mg each of loose coated sol-gel UO_2 particles using natural uranium. The

*Great Lakes Carbon Co.
†R. T. Vanderbilt Co.
‡Allied Chemical Co.

Table 6. Properties of ORNL Bonded Rods for HT-31

Property	Slug-Injected ORNL-1 (2-5)	Extruded ORNL-2 (J1-179-4)	
		Before HT-23	After HT-23[a]
Dimensions, mm (in.)			
Average OD	10.155 (0.3998)	10.165 (0.4002)	9.835 (0.3872)
Average ID	3.30 (0.130)	3.33 (0.131)	3.23 (0.127)
Average length	50.084 (1.9718)	50.813 (2.0005)	48.618 (1.9141)
Matrix density, g/cm^3	0.41	1.62	
Particle loading, vol %	57.4	34.8	
Electrical resistivity at 295 K, Ω-m	79.26	29.46	40.15

[a]After two cycles in HFIR capsule HT-23 and after graphite fixtures had been machined from bottom and top of specimen.

particles in U-16 were Biso-coated and in U-17 Triso-coated. The reason for using $^{238}UO_2$ instead of $^{235}UO_2$ was that a larger supply could be irradiated without excessive local heating.

The three specimens from LASL are extruded rods and are described in ref. 2. Each of these bonded rods contained 13.9 kg/m^3 of 6.5%-enriched uranium and 41.3 kg/m^3 of thorium and had maximum dimensions of 9.78 mm in diameter by 21.34 mm in length (0.385 by 0.840 in.). The 6.5%-enriched uranium was for heat generation early in the irradiation.

The lower half of the capsule contained loose coated particles in graphite holders and in indicated end plugs. The uranium positions were occupied by ORNL weak-acid-resin-derived (WAR) particles (6.53% enriched) to provide heat generation early in the irradiation. Details on these particles are given in Tables 3, 4, and 5. The outer low-temperature isotropic (LTI) coating was burned off many particles (see Table 3), so a sufficient number of particles could be accommodated in the graphite holders to provide the necessary heat generation.

The thorium positions were occupied by loose coated ThO_2 particles (both Biso- and Triso-coated) fabricated by GA. Detailed descriptions of these particles are given in ref. 1.

3. CAPSULE OPERATION

Capsule HT-31 was inserted into HFIR target position G-5 on March 14, 1976, and removed on June 16, 1976, after 2146.56 h at 100 MW reactor power and delivered to the hot cells for postirradiation examination on June 18, 1976 (Table 7). The thermal and fast fluences and burnups for the capsule are presented in Tables 8 and 9, respectively.

Table 7. Irradiation History of HT-31

Cycle	Begin		End		Irradiation Time[a] (h)	
	Time	Date	Time	Date	During Cycle	Accumulated
130	1732	3/14/76	2354	4/6/76	557.76	557.76
131	2124	4/7/76	2312	4/30/76	552.48	1110.24
132	2142	5/1/76	0800	5/22/76	489.60	1599.84
133	2211	5/23/76	1240	6/16/76	546.72	2146.56

[a]At 100 MW Reactor Power.

4. THERMAL ANALYSIS

Time-temperature histories for the GA loose ThO_2 particles irradiated in the lower two graphite magazines of HT-31 are shown in Figs. 2 and 3 for the high-temperature region, and Figs. 4 and 5 for the low-temperature region. Temperature histories were calculated with the HTCAP1 thermal modeling code (Modified version of the HTCAP code[5]). Each figure describes the maximum particle surface temperature, graphite holder annulus temperature, and power generated per particle as functions of time from the beginning of irradiation.

The above figures illustrate that the irradiation temperatures in this HT capsule were not constant. Only the last two cycles in the high-temperature magazine and the last cycle in the low-temperature magazine show any indication of constant temperature. Table 10 describes the average particle surface temperatures and power histories for each ThO_2 particle type, for both magazines, during the last irradiation cycle.

Table 8. Thermal and Fast Fluences for HT-31

Specimen	Distance From HMP to Specimen Centerline		Flux, n/m^2 s		Fluence, n/m^2	
	(mm)	(in.)	Thermal <0.414 eV	Fast >0.18 MeV	Thermal	Fast
			$\times 10^{19}$	$\times 10^{19}$	$\times 10^{26}$	$\times 10^{25}$
Crucible-1	246.38	9.700	1.33	0.482	1.03	3.72
ORNL-1	196.85	7.750	1.76	0.733	1.36	5.66
ORNL-2	139.70	5.500	2.15	0.950	1.66	7.34
U-16	92.10	3.626	2.46	1.075	1.90	8.31
U-17	84.94	3.344	2.50	1.095	1.93	8.46
LASL-1	70.59	2.779	2.58	1.120	1.99	8.65
LASL-2	49.05	1.931	2.68	1.150	2.07	8.89
LASL-3	27.53	1.084	2.77	1.165	2.14	9.00
27	−20.35	−0.801	2.80	1.170	2.16	9.04
28	−27.53	−1.084	2.77	1.165	2.14	9.00
29	−34.70	−1.366	2.75	1.160	2.13	8.96
30	−41.88	−1.649	2.72	1.155	2.10	8.93
31	−49.05	−1.931	2.68	1.150	2.07	8.89
32	−56.24	−2.214	2.65	1.140	2.05	8.81
33	−63.40	−2.496	2.62	1.130	2.02	8.73
34	−70.59	−2.779	2.58	1.120	1.99	8.65
35	−77.75	−3.061	2.55	1.108	1.97	8.56
36	−84.94	−3.344	2.50	1.095	1.93	8.46
37	−92.10	−3.626	2.46	1.075	1.90	8.31
38	−99.29	−3.909	2.41	1.060	1.86	8.19
39	−106.65	−4.199	2.36	1.040	1.82	8.04
40	−147.35	−5.801	2.10	0.930	1.62	7.19
41	−154.53	−6.084	2.06	0.909	1.59	7.02
42	−161.70	−6.366	2.00	0.880	1.55	6.80
43	−168.88	−6.649	1.94	0.850	1.50	6.57
44	−176.05	−6.931	1.90	0.820	1.47	6.34
45	−183.24	−7.214	1.86	0.790	1.44	6.10
46	−190.40	−7.496	1.80	0.760	1.39	5.87
47	−197.59	−7.779	1.74	0.730	1.34	5.64
48	−204.75	−8.061	1.68	0.695	1.30	5.37
49	−211.94	−8.344	1.62	0.665	1.25	5.14
50	−219.10	−8.626	1.56	0.640	1.21	4.95
51	−226.29	−8.909	1.50	0.595	1.16	4.60
52	−233.65	−9.199	1.44	0.560	1.11	4.33

Table 9. Capsule HT-31 Fuel Specimen Burnups (FIMA)

Specimen	Burnups (% FIMA)		
	^{235}U	^{238}U	^{232}Th
U-16	84.71	17.40	
U-17	84.73	17.60	
LASL-1	84.77	18.00	8.59
LASL-2	84.80	18.30	8.75
LASL-3	84.83	18.50	8.88
27			8.91
28	84.83	18.50	
29			8.85
30			8.80
31	84.80	18.30	
32			8.69
33			8.62
34	84.77	18.00	
35			8.49
36			8.40
37	84.71	17.40	
38			8.21
39	84.67	17.00	
40			7.21
41	84.50	15.19	
42			6.90
43			6.70
44	84.41	14.10	
45			6.30
46			6.10
47	84.32	12.90	
48			5.62
49			5.40
50	84.22	11.50	
51			4.90
52	84.16	10.60	

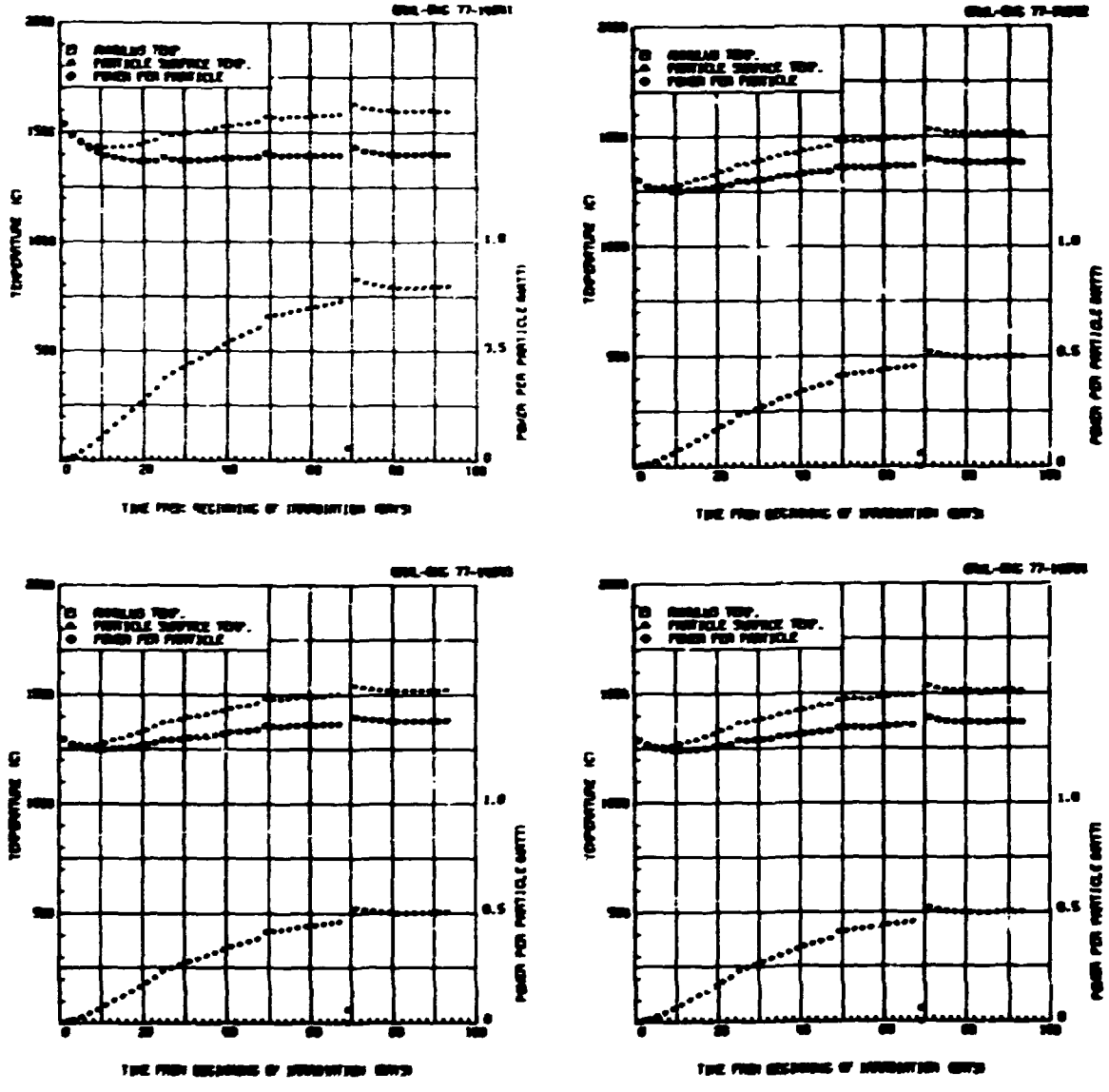

Fig. 2. Time-Temperature and Time-Power Histories for GA ThO_2 Particles Irradiated in the High-Temperature Magazine of HT-31. (a) Holder 27, batch 05-0160-006, 872 μm particle diameter. (b) Holder 29, 08-0161-002, 836 μm. (c) Holder 30, 10-0161-002, 824 μm. (d) Holder 32, 09-0161-002, 819 μm.

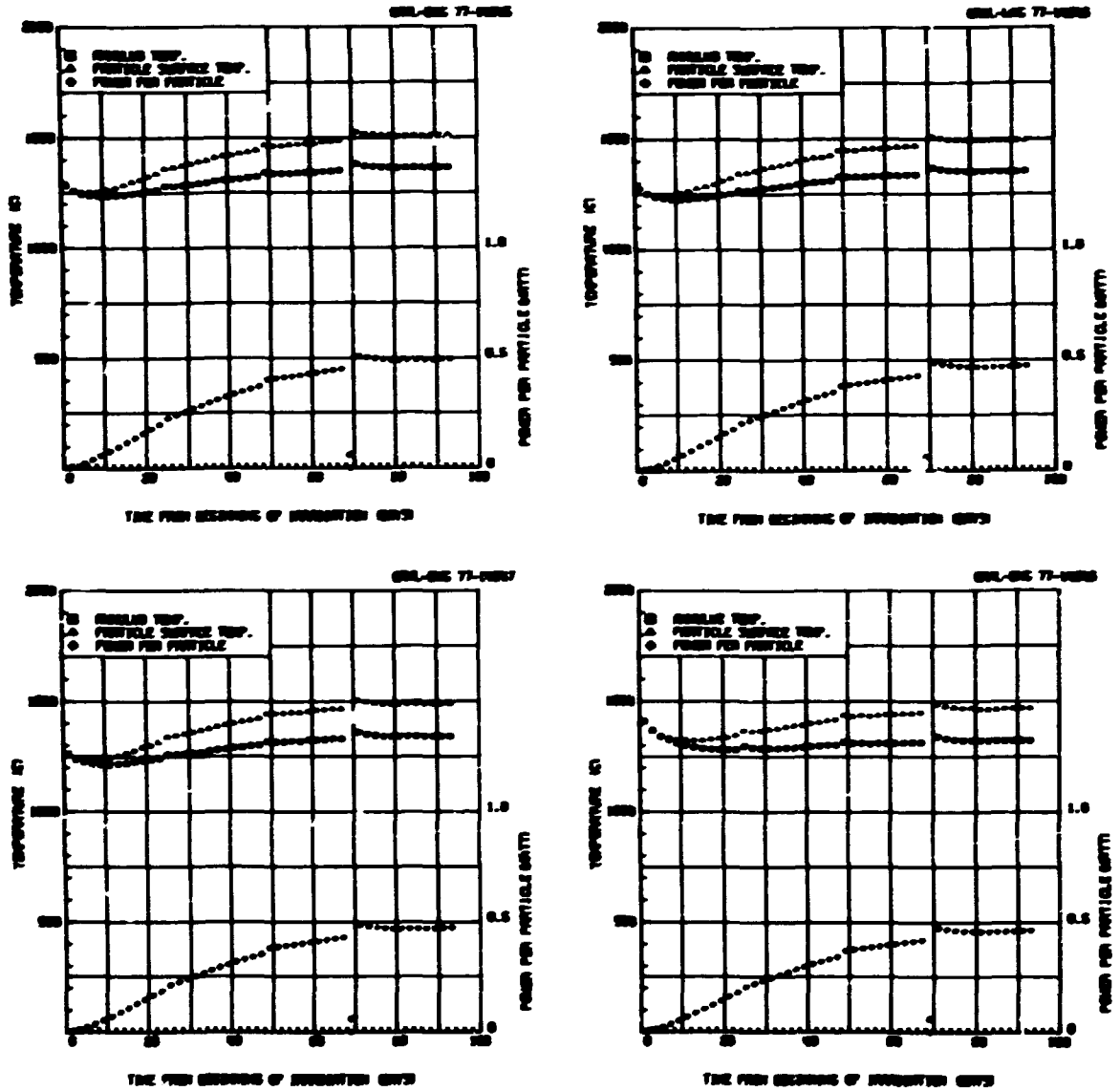

Fig. 3. Time-Temperature and Time-Power Histories for GA ThO_2 Particles Irradiated in the High-Temperature Magazine of HT-31. (a) Holder 33, batch 07-0261-002, 821 μm particle diameter. (b) Holder 35, 07-0161-002, 823 μm. (c) Holder 36, 05-0261-002, 812 μm. (d) Holder 38, 06-0161-002, 823 μm.

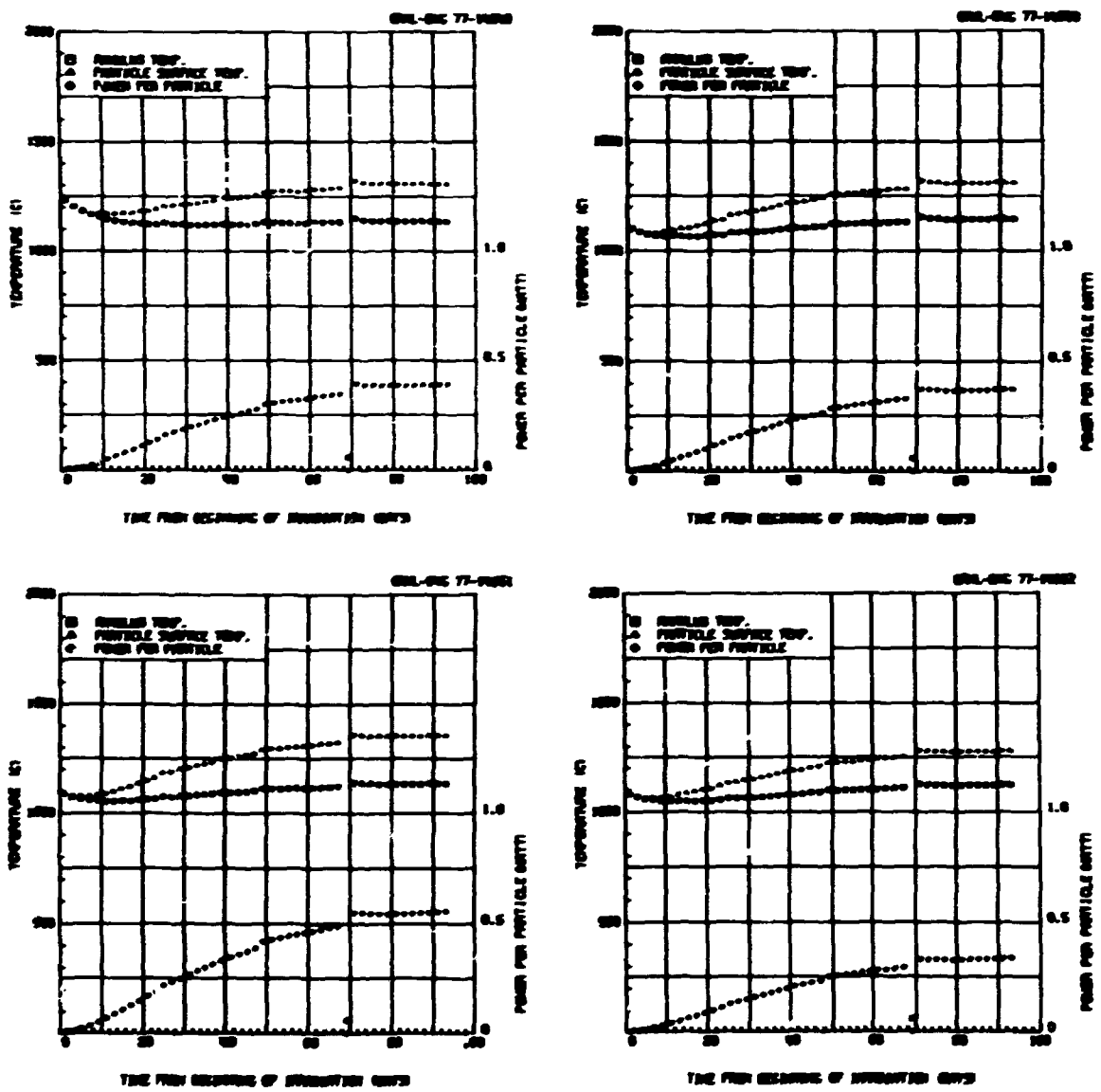

Fig. 4. Time-Temperature and Time-Power Histories for GA ThO_2 Particles Irradiated in the Low-Temperature Magazine of HT-31. (a) Holder 40, batch 10-0161-001, 829 μm particle diameter. (b) Holder 42, 09-0161-001, 823 μm. (c) Holder 43, 05-0160-005, 873 μm. (d) Holder 45, 07-0261-001, 820 μm.

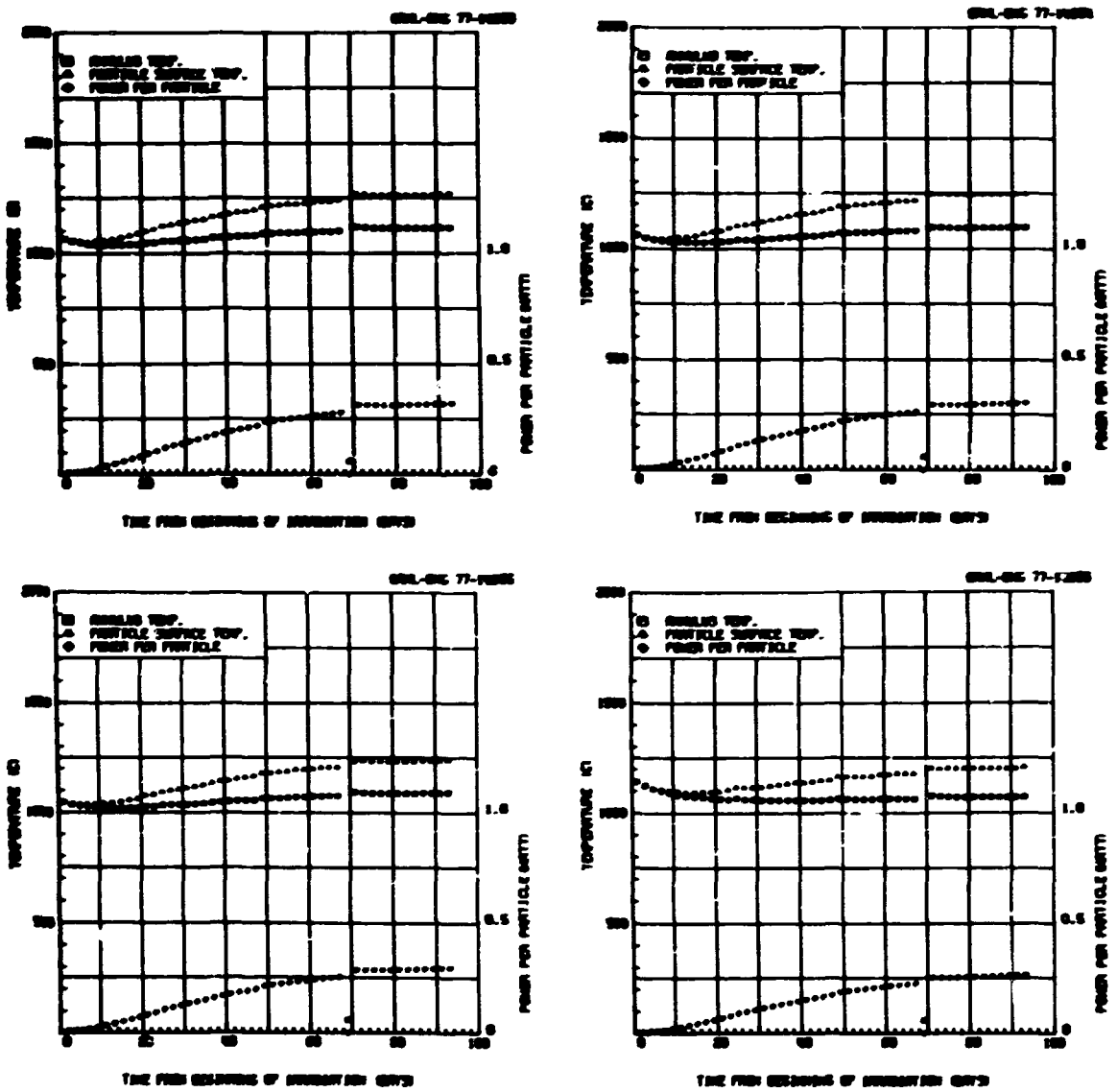

Fig. 5. Time-Temperature and Time-Power Histories for GA ThO_2 Particles Irradiated in the Low-Temperature Magazine of HT-31. (a) Holder 46, batch 07-0161-001, 816 μm particle diameter. (b) Holder 48, 06-0261-001, 813 μm. (c) Holder 49, 06-0161-001, 819 μm. (d) Holder 51, 08-0161-001, 836 μm.

Table 10. Operating History for GA ThO_2 Loose Particles During Irradiation Cycle 142 of Capsule HT-31

GA Particle Type	Diameter (μm)	Holder	Av. Surface Temperature (°C)	Av. Power Generation (W)
05-0160-006	872	27	1600	0.80
08-0161-002	836	29	1520	0.50
10-0161-002	824	30	1520	0.50
09-0161-002	819	32	1515	0.50
07-0261-002	821	33	1510	0.47
07-0161-002	823	35	1495	0.47
06-0261-002	812	36	1490	0.47
06-0161-002	823	38	1470	0.46
10-0161-001	829	40	1310	0.39
09-0161-001	823	42	1310	0.37
05-0160-005	873	43	1350	0.55
07-0261-001	820	45	1275	0.33
07-0161-001	816	46	1265	0.31
06-0261-001	813	48	1245	0.35
06-0161-001	819	49	1230	0.29
08-0161-001	836	51	1200	0.26

In each magazine the general trend is for the power generated per particle and temperature to follow the HFIR flux profile with the peak nearest the reactor horizontal midplane and decreasing to a minimum at the ends of the magazine.

One ThO_2 particle type, 6252-05-0160, contained a nominal 500-μm kernel (while all other particle types were 450 μm or less in diameter). Consequently this particle type generated more heat and thus had a higher surface temperature, 1600°C in the high-temperature region and 1350°C in the low-temperature region. These temperatures are illustrated in Table 10 for holders 27 and 43 and Figs. 2(a) and 4(c).

Time-temperature histories were also obtained for ORNL-produced fissile particles used as drivers in the lower magazines. These particles

were also irradiated loose in graphite holders similar to those used with the ThO_2 particles. In each magazine, five holders contained Triso-coated WAR driver particles, batch OR-2248. These particles were 6.5% enriched uranium and were used for heat generation at the beginning of irradiation. Table 11 describes the operating temperature history of the uranium driver particles for each HFIR cycle.

Table 11. Maximum Particle Surface Temperatures for Driver Particle Batch OR-2248 Irradiated in HT-31

Holder	Cycle 130	Cycle 131	Cycle 132	Cycle 133
28	1557–1387	1406–1402	1420–1409	1445–1415
31	1546–1377	1392–1391	1407–1399	1434–1402
34	1532–1363	1379–1375	1393–1385	1418–1388
37	1513–1347	1359–1352	1371–1363	1398–1369
39	1476–1289	1306–1281	1293–1279	1305–1279
41	1356–1202	1214–1194	1208–1200	1221–1201
44	1330–1183	1189–1171	1182–1177	1197–1183
47	1297–1163	1169–1148	1157–1152	1166–1155
50	1266–1143	1149–1123	1134–1124	1144–1130
52	1229–1107	1110–1074	1080–1069	1078–1064

Particle temperatures were high at the beginning of irradiation while ^{235}U was still present (cycle 130). As the ^{235}U was burned up the temperature range decreased as illustrated for cycles 131, 132, and 133. Here the primary source of heat for the driver particles was fissioning of plutonium produced from the ^{238}U.

5. POSTIRRADIATION EXAMINATION

5.1 Disassembly and Visual Examination

The capsule was sectioned and the contents were removed intact and in good condition.

Crucible 1 appeared normal and was prepared for removal to another facility for permeability measurements. Bonded rods ORNL-1 and -2 appeared sooty and were prepared for transfer to the Physical Properties Group for physical measurements. Holders U-16 and -17 and the LASL rods were removed in good condition. Further analysis of the results on the LASL rods is reported in ref. 2.

The loose coated ThO_2 particles from the lower half of the capsule were removed from their respective graphite holders without incident. A representative from GA was present during disassembly of these holders. Further analysis of the results on the GA fuel particles is reported in ref. 6.

The loose WAR driver particles were also removed from their respective graphite holders. (These particles did not have outer LTI coatings.) With the exception of the particles from holder 52, the particles appeared to be in poor condition. In many cases the particles had bonded to one another, and many could not be removed from the graphite holders. Broken coatings and fragments were observed, but no accurate failure count could be made because we could not remove all the particles. The surfaces of the particles appeared to be very rough and discolored (Fig. 6). Further discussion on these particles will be presented in a following section. The particles from holder 52 appeared to be in excellent condition with shiny surfaces (typical of SiC).

5.2 Dimensional Inspection

The bonded rods ORNL-1 and -2 were dimensionally inspected and the data are summarized in Table 12. The rods were transmitted to the Physical Properties Group at ORNL, where the thermal expansivities and conductivities of these rods were measured and reported.[7]

5.3 Permeability Measurements

The inert coated particles (batch OR-2294-HT) contained in Crucible 1 were used for measurements of the coating Ne/He permeability. This value gives a measure of the permeability of the pyrocarbon coating for inert

Fig. 6. Representative Appearance of Loose Coated Driver Particles (with No Outer LTI Coating) After Irradiation Sample is from Holder 41. 20×.

Table 12. Dimensional Changes in Rods Irradiated for Thermal Property Measurement

Dimension	Average Value, mm (in.)		Change, %	
	ORNL 1	ORNL 2	ORNL 1	ORNL 2
Average OD	9.774 (0.3848)	10.053 (0.3958)	−3.88	−1.10
Average ID	3.250 (0.128)	3.230 (0.127)	−1.5	−3.0
Average length	48.077 (1.8928)	48.951 (1.9272)	−4.01	−3.52

[a]Changes given for OD and ID radial.

[b]Total change from preirradiation values.

gases. The results, which are shown in Table 13, indicate that the permeability of the pyrocarbon coatings decreased with fast-neutron fluence (0.18 MeV). While tentative, these results have been confirmed in subsequent irradiation experiments for the pyrocarbon coatings of particles with inert kernels.[8]

Table 13. Permeability of Irradiated Inert Fuel Particles from HT-31

Batch	Fast-Neutron Fluence, >0.18 MeV (n/m^2)	Temperature (°C)	Content, mol/fuel particle		Se/He
			Helium	Neon	
OR-2294-HT (inerts)			1.07×10^{-14}	0.24×10^{-14}	0.22
OR-2294-HT (inerts)	4.4×10^{25}	950	5.10	0.13	0.12
OR-2261-HT (included for comparison)			1.42	0.30	0.21

5.4 Gas Pressure Measurements

Both Biso- and Triso-coated natural UO_2 kernels (0.7% ^{235}U) were irradiated to investigate the chemical effects of plutonium fissions on oxygen release in UO_2. The kernels were 97%-dense sol-gel UO_2 and were selected from a large batch by microsieving to give an average kernel diameter with a very small standard deviation. Tables 3, 4, and 5 describe the particles.

The theoretical fractions of ^{95}Zr, ^{106}Ru, ^{137}Cs, and ^{144}Ce left at the end of irradiation were calculated by taking into account the time-dependent fission rates of ^{235}U, ^{239}Pu, and ^{241}Pu (Table 14). Contributions to the fraction of total fissions by each of these three isotopes were also calculated:

Isotope	Fraction of Total Fissions (%)
^{235}U	4.7
^{239}Pu	71.2
^{241}Pu	24.1

Based on these calculations and the results from gamma spectrometry of six particles from each batch, burnups were determined (Table 14). Details of

Table 14. Theoretical Fraction of Selected Isotopes Left at the End of Irradiation and the Burnups based on Gamma Spectrometry of These Isotopes

Isotope	Theoretical Fraction Left at End of Irradiation (%)	Burnup Based on Isotope Gamma Spectrometry (% FIMA)	
		U-16, Biso-Coated (Batch OR-2511-H)	U-17, Triso-Coated (Batch OR-2533-H)
^{95}Zr	0.676	11.68	11.88
^{106}Ru	0.929	12.71	13.18
^{137}Cs	0.998	13.17	13.68
^{144}Ce	0.910	11.36	11.50

these type of calculations are given in ref. 9. One Biso-coated particle lost about 50% of the ^{137}Cs content so that the ^{137}Cs burnup is based on five particles. The results from the ^{137}Cs indicate a higher burnup than do those from the other three isotopes, a phenomenon noted earlier in other ThO_2 irradiations.[3,9]

The irradiated particles were individually heated at a given temperature, broken, and measured for CO and Kr + Xe contents.[9,10] The experimental results are given in Table 15. It is clear from a comparison of the Biso-vs-Triso results for oxygen per fission (O/f) and Kr + Xe per fission [(Kr + Xe)/f] that the Biso-coated particles were permeable to CO, Xe, and Kr. The Triso-coated particles contained the gases with the observed (Kr + Xe)/f comparable to the theoretical value of 0.32.

The release of oxygen as a result of the plutonium fission is commonly expected to be higher than that for uranium fission.[11-13] However, the present experiments, as well as those of European measurements[11,12] on irradiated low-enriched uranium, revealed an oxygen release that was usually well below the thermodynamically calculated minimum value of about 0.57 oxygen atom per fission (O/f). The present Triso-coated particle results approach that value at 1600°C (Table 15), but the lower temperature European results[11,12] are for particles with considerably fewer total fissions. In general, one expects O/f = 0.57 and finds 0.2 to 0.3 at

Table 15. Contents of CO and Kr + Xe in Irradiated Natural UO_2 Particles

Equilibration Temperature (°C)	Equilibration Time (h)	Gas Found (nmol)		Moles per Fission	
		CO	Kr + Xe	O/f	(Kr + Xe)/f
U-16 (Batch OR-2511-H, Biso-Coated)					
870	163.0	34.2	35.6	0.216	0.226
1000	143.3	45.8	36.7	0.290	0.232
1200	92.6	58.8	36.9	0.372	0.233
1400	89.0	56.7	35.6	0.359	0.226
1635	19.5	68.9	36.8	0.436	0.233
U-17 (Batch OR-2533-H, T iso-Coated)					
1400	6.8	67.4	55.2	0.422	0.350
1600	7.3	88.5	52.1	0.554	0.331

7% FIMA. Thus, the difference of about 0.4 O/f is equivalent to a deficiency of 0.4 × 0.07 = 0.028 oxygen atom per metal atom; this could be accommodated by an equivalent increase in the O/U ratio. This increase can be shown to be impossible with pure UO_2, but could possibly occur as a result of the known[14] solid solution of SrO and the rare earth oxides in UO_2. However, no data are known on the effects of solid solution SrO on the O/U ratio. Data on the rare-earth oxide solutions are summarized in ref. 10 but are not accurate enough to predict an increase of about 0.03 in the O/U ratio. Thus the present results are inconclusive, but do agree with previous experiments.

5.5 Driver Particle Examination

Originally, the low-enriched uranium (LEU) driver particles did not represent an integral part of the experiment, but because of the new interest in LEU feul (prompted by recent government policy changes), examination of these fuels became important. However, these particles were irradiated without an outer LTI coating, which affected their performance. The outer LTI coatings had been burned off so that a sufficient number of

particles could be accomodated in the loose particle graphite crucibles to obtain the necessary fuel loadings. However, it was hoped that successful irradiation of these particles would prove to be a scoping experiment for a new fissile particle design (i.e., Triso-coated without an outer LTI).

During unloading of the graphite crucibles from the high-temperature region, many of the particles were stuck in the crucibles and could not be removed. The particles that were removed showed extensive degradation of the SiC coating, similar to that shown in Fig. 6. The particles contained in the low-temperature crucibles were more easily removed (with the exception of crucible 41) but also showed some degradation of the SiC coating. The particles from crucibles 50 and 52 showed no apparent SiC degradation.

Examination of graphite crucible 41 (with particles stuck in it) using the shielded scanning electron microscope (SEM) showed that the particles were bonded to the graphite, and a well-defined crystal structure was observed on the graphite surface (Fig. 7). Other studies[15–17] have shown that in a neutral or reducing atmosphere, bare SiC can degrade through the evaporation of silicon, leaving a porous carbon layer. Measurements of the sublimation of SiC under equilibrium conditions have shown that the most important gaseous species is silicon. The decomposition rate of β-SiC crystals (the type deposited on HTGR fuel particles) was measured and fitted to the following equation:

$$k = 2.95 \times 10^{13} \exp(-56{,}252/T) , \qquad (1)$$

where k is the decomposition rate in $\mu g/m^2$ s and T is the temperature in K. Particles from crucible 41 (shown in Fig. 6) operated at a time-averaged particle surface temperature of about 1215°C, and with Eq. (1) a rate of 1.13 ng/m^2 s can be calculated. This amounts to an effective decrease in the SiC thickness of about 0.01 μm. However, the appearance in Fig. 7 would indicate that more SiC was degraded. This discrepancy can be partially accounted for by the particle surface temperature having reached as high as 1350°C early in irradiation, and considerably more SiC degradation should have occurred. However, at 1350°C the decomposition rate is 2.62 ng/m^2 s, which would amount to an effective decrease in the SiC thickness of about 0.2 μm provided that 1350°C was the average temperature

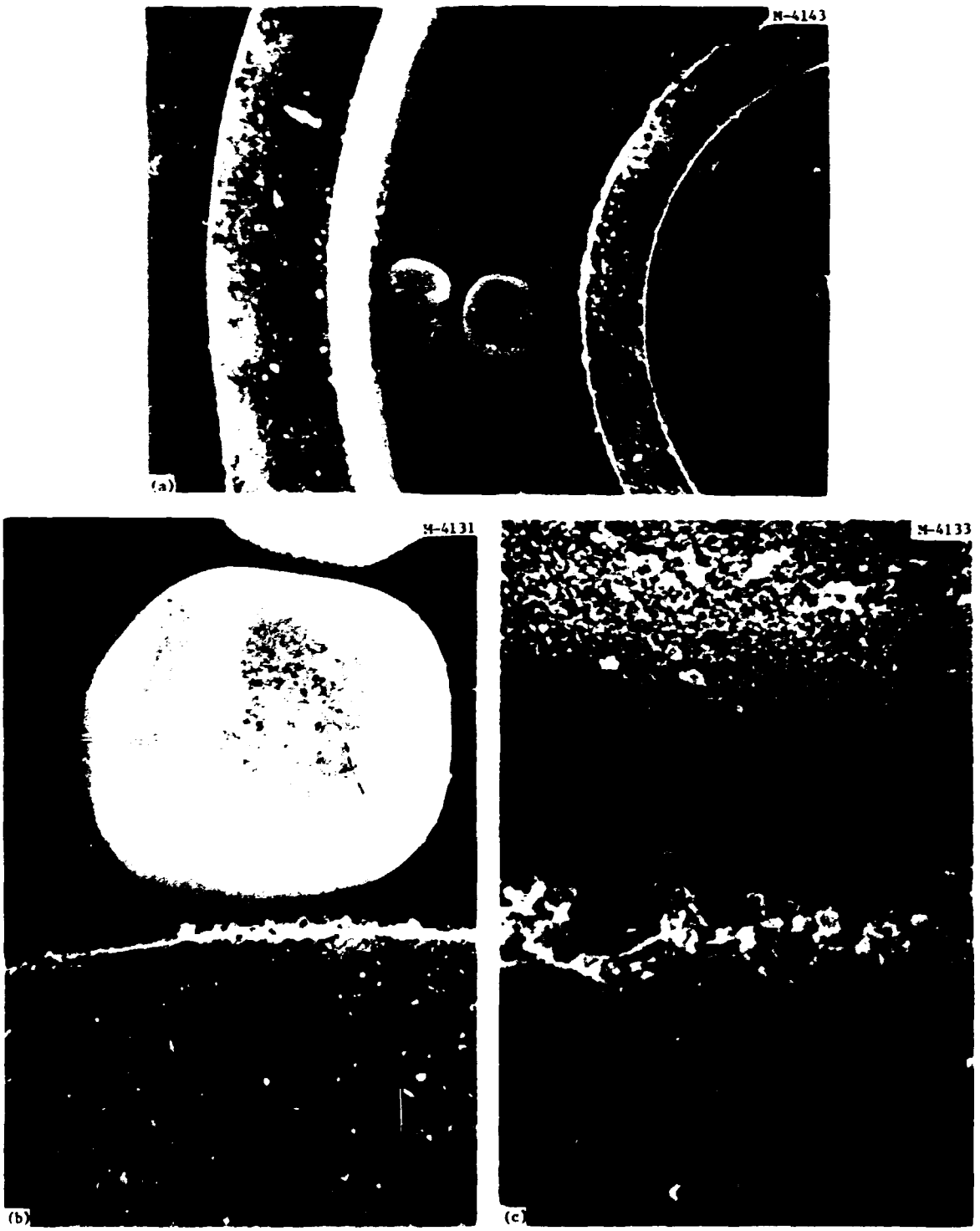

Fig. 7. Particle Adhering to Crucible 41. (a) 13, (b) 70, and (c) 340×. At 340× crystal growth from the graphite surface is easily observed. Reduced 68.5%.

during the irradiation. The amount of degradation observed in crucible 41 appeared to be about 0.5 μm, which would indicate a time-averaged temperature of about 1390°C. Evidently, either the particle surface temperatures were higher than we had calculated or the decomposition rates were higher than predicted by Eq. (1).

Examination by the SEM of one of the particles removed from crucible 28 (Fig. 8) showed extensive SiC degradation. One area shown (b) is believed to have been where two particles were in contact and the SiC sublimation rate was lower than over the rest of the particle. Using the time-averaged particle surface temperature for crucible 28 (~1415°C), a SiC decomposition rate of 99.3 ng/m^2 s can be calculated with Eq. (1). This amounts to an effective decrease in SiC thickness of about 0.8 μm. However, the particle surface temperature was as high as 1555°C early in irradiation. The calculated decomposition rate at this temperature was 1.28 $\mu g/m^2$ s. The amount of SiC decomposition was not estimated.

These results showed that the performance of the driver particles without an OLTI coating was questionable because of SiC sublimation. Consequently, further examination of these LEU driver particles was stopped. This decision was also based on the availability for examination of other HT-capsules (e.g., HT-33)[18] containing LEU driver particles that were irradiated with OLTI coatings. Although SiC sublimation was evidently a problem in the capsule, the particles from crucible 52 appeared to be in excellent condition, with no apparent SiC degradation, and may be used in future testing of LEU fuel. (In fact, particles from crucible 52 were given to GA for tests on plutonium volatility in LEU fuel particles.)

5.6 Electron Microprobe Examination of Normal UO_2 Particles

5.6.1 Biso-Coated Sol-Gel Particles

The sol-gel UO_2 particles were irradiated as loose particles, so we could mount them individually and metallographically polish them. A cross-section of a Biso-coated particle is shown in Fig. 9. The particles appeared to be in good condition, but, as discussed in Sect. 5.5, the coatings on these particles were probably permeable to gases during

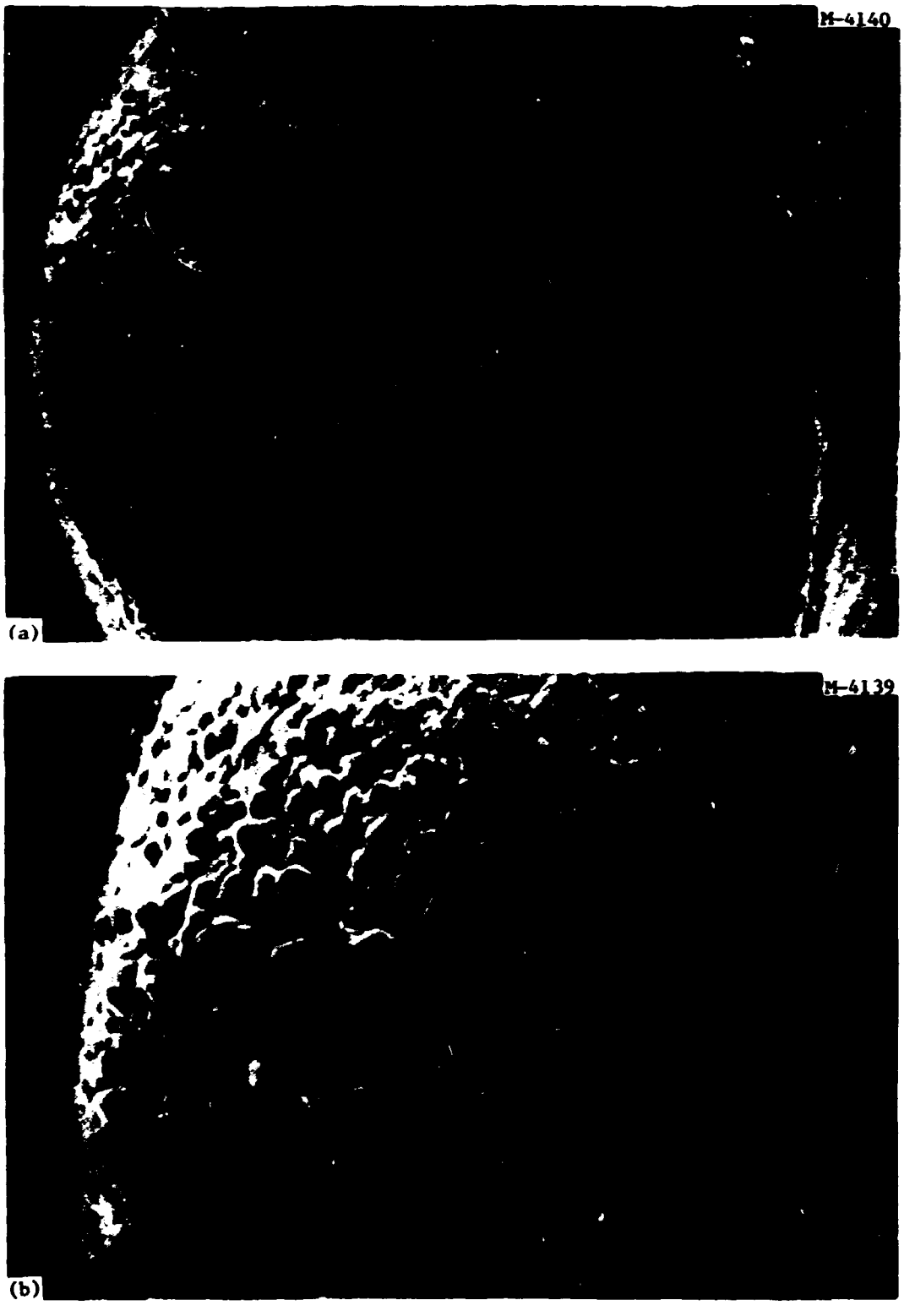

Fig. 8. Single Particle from Crucible 28 Showing Severe Degradation of SiC. (a) 200×. (b) 365×. Area shown in (b) is probably where this particle rested against another. Reduced 88%.

R-75443

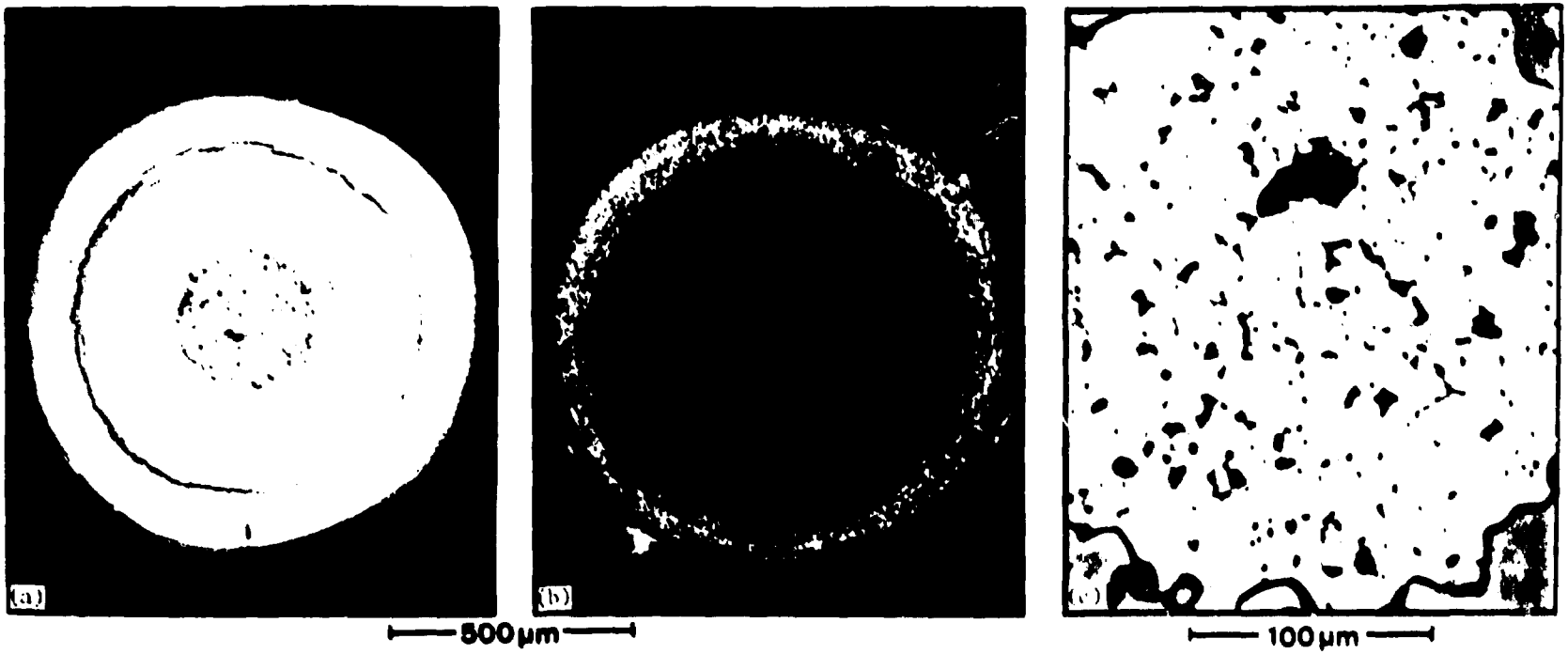

Fig. 9. Single Biso-Coated Sol-Gel Particle. (a) Bright field. (b) Polarized light. (c) High magnification of kernel, showing numerous phases present.

irradiation. Observations on the kernel [Fig. 9(c)] revealed numerous phases at the grain boundaries; these included fission gas bubbles, bright metallic inclusions, and gray ceramic inclusions. Close examination of the OLTI coating showed a thin layer of bright material (not optically active under polarized light), which covered nearly the entire outer surface (Fig. 10).

The shielded electron microprobe showed that the thin layer of material was zirconium (Fig. 11). The only source of zirconium in the capsule (besides the fission products) was the wafers inserted between the graphite crucibles, which are included as oxygen getters during irradiation. In a previous HT-capsule,[19] chemical attack of fuel rods by zirconium had been observed and a similar situation could have occurred.

Also shown in Fig. 11 is the cesium distribution in the particle. It had migrated out of the kernel and into the buffer and LTI coating. Cesium was the only fission product in the pyrocarbon coatings in sufficient concentration to produce an appreciable x-ray display.

Close examination of the kernel showed that uranium, plutonium, and the rare earth fission products Nd, La, and Pr (Nd representative of La and Pr) were evenly distributed in the residual kernel matrix presumably as oxides (Fig. 12). Similar results have been reported[20] with highly enriched uranium (HEU) sol-gel UO_2 particles.

Cerium, which usually behaves like the other rare earth fission products in HTGR particles,[20,21] was observed in the residual kernel matrix and heavily concentrated in the gray ceramic phases (Fig. 13). Associated with the cerium in the ceramic phases were strontium and barium. Similar inclusions have been observed[22] in mixed uranium-plutonium fuel pellets irradiated in a fast neutron flux. The zirconium, which is sometimes present in the ceramic inclusions,[21,23] was found distributed throughout the residual kernel matrix without any apparent concentration in the inclusions.

The metallic inclusions were composed of Mo, Ru, Pd, Rh, and Tc (Fig. 14). In addition, minor concentrations of each of the elements were distributed in the redisual kernel matrix. Similar inclusions have been observed in HTGR fuel particles with high oxygen contents[21,24] and mixed uranium-plutonium fuel pellets.[22] Palladium recently has become of major

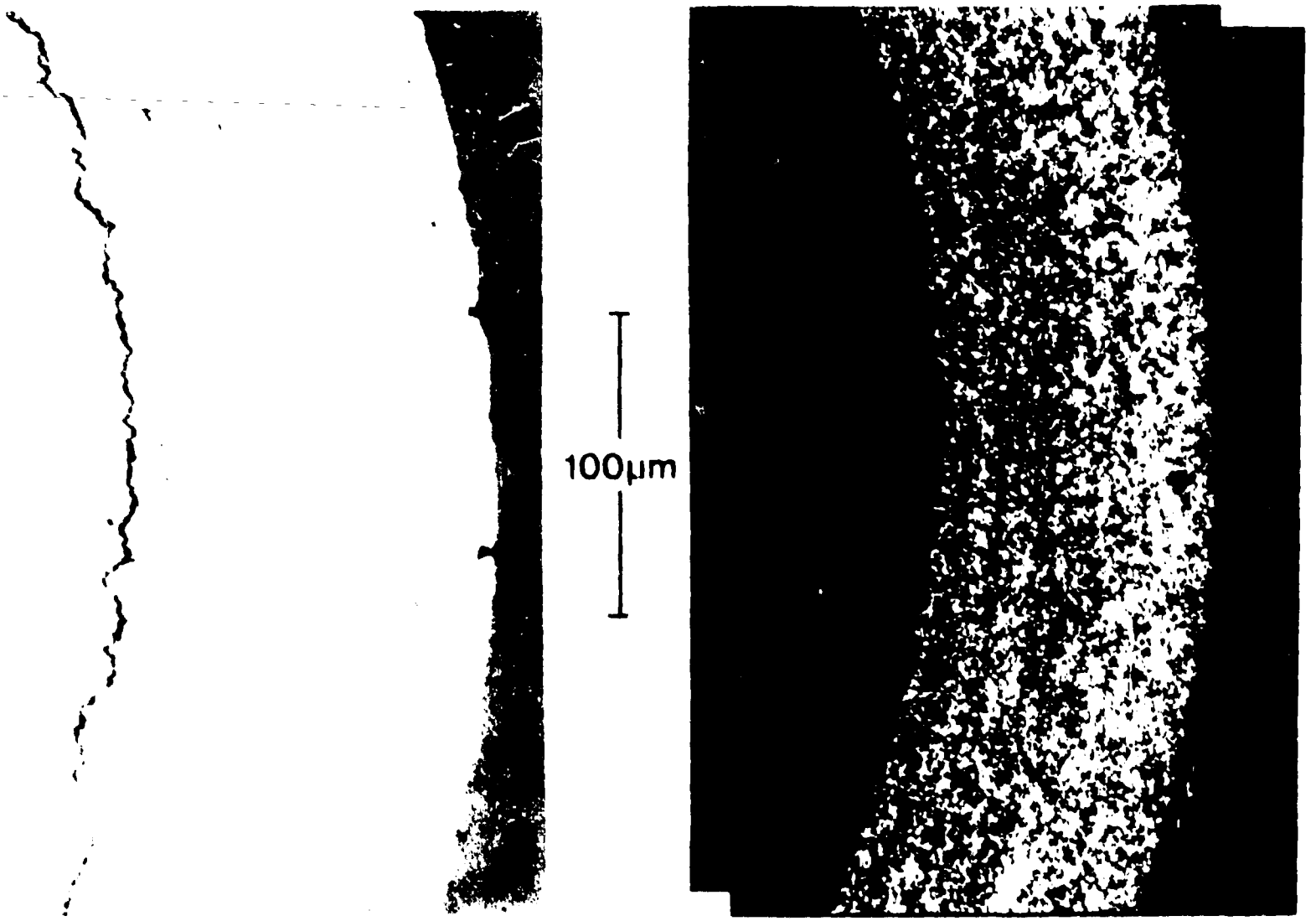

Fig. 10. Outer Surface of BISO-Coated Fuel Particle Showing Layer of Zirconium. (a) Bright Field. (b) Polarized Light.

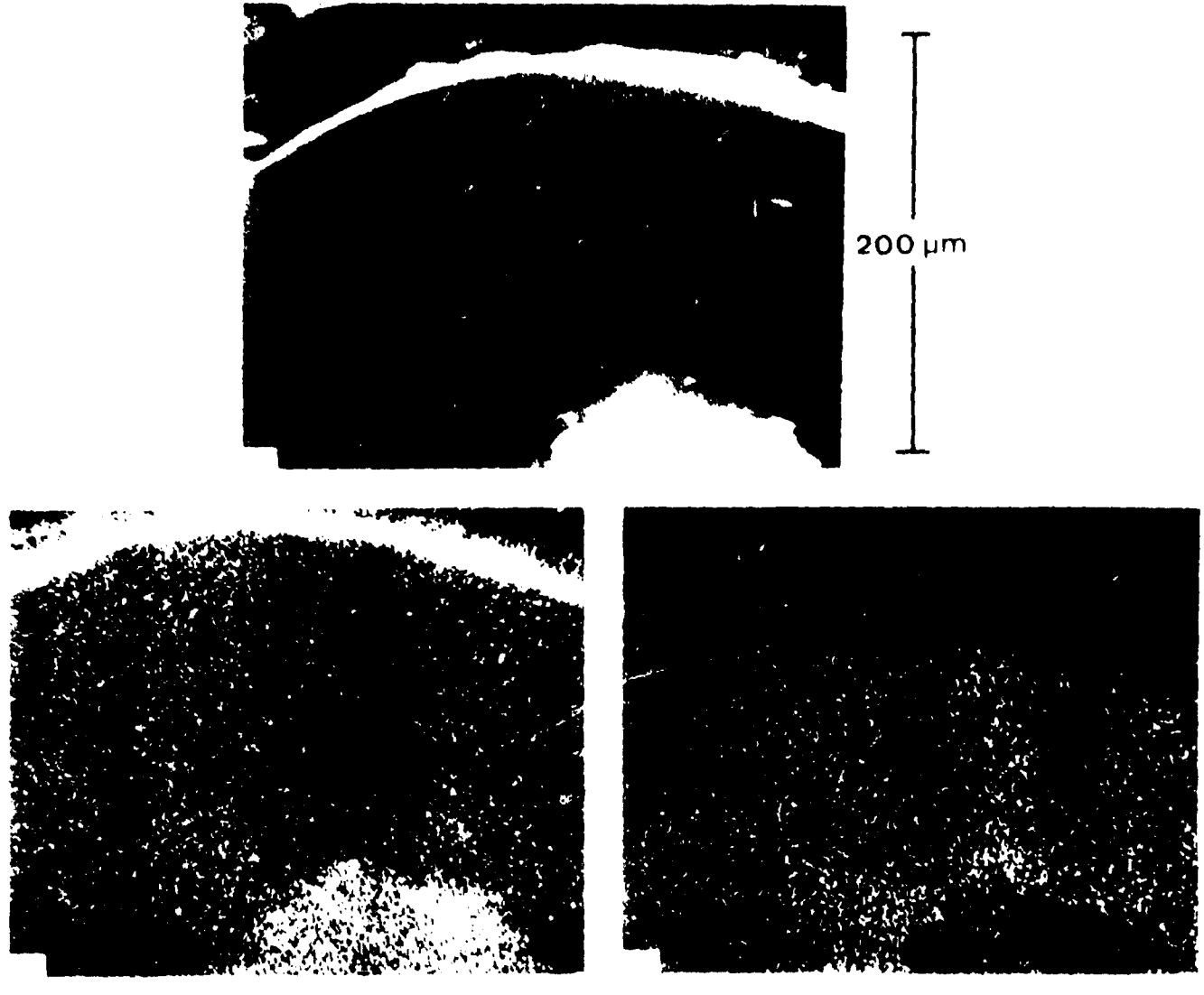

Fig. 11. Electron Micrograph Series [illegible] Particles as Zirconium. (a) Backscattered electron image.

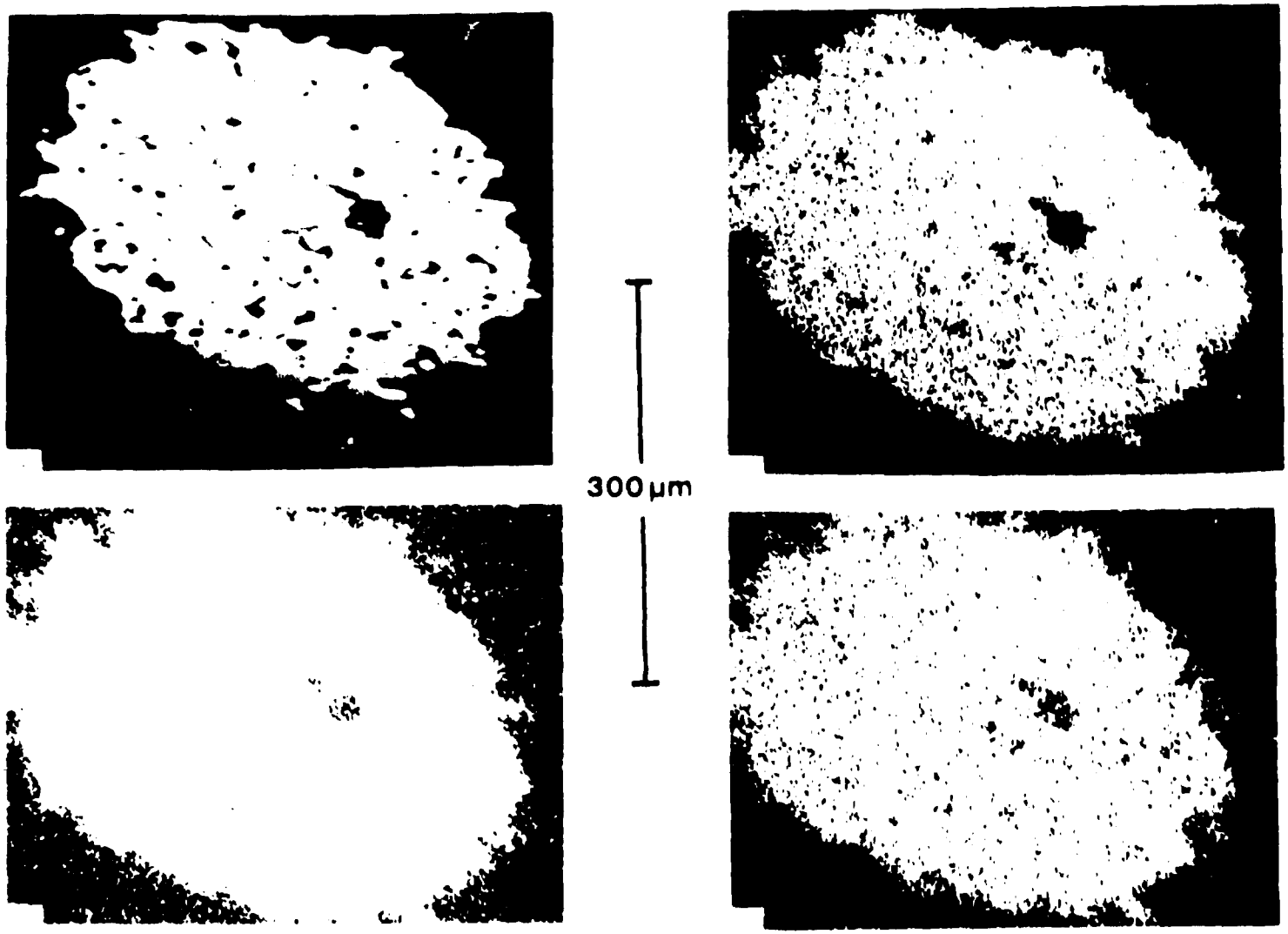

Fig. 12. Electron microprobe displays of kernel of Biso-coated Sol-Gel Particles. (a) Backscattered electron image. (b) U M$_\alpha$. (c) Pu M$_\alpha$. (d) Nd L$_\alpha$.

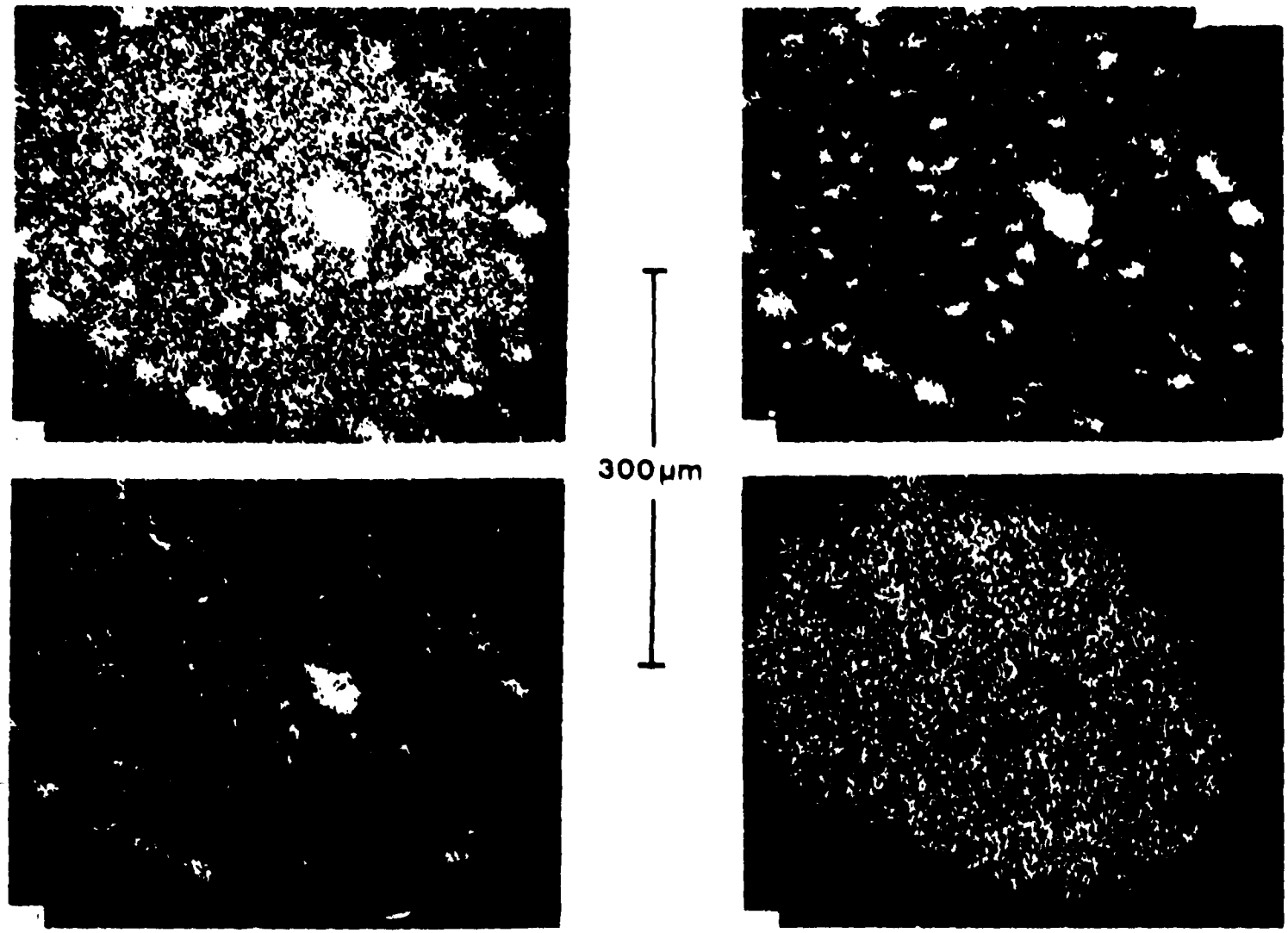

Fig. 13. Electron Microprobe X-ray Displays of Kernel of Biso-Coated Sol-Gel Particle. Same orientation as Fig. 12. (a) Ce Lα. (b) Ba Lα. (c) Sr Lα. (d) Zr Lα.

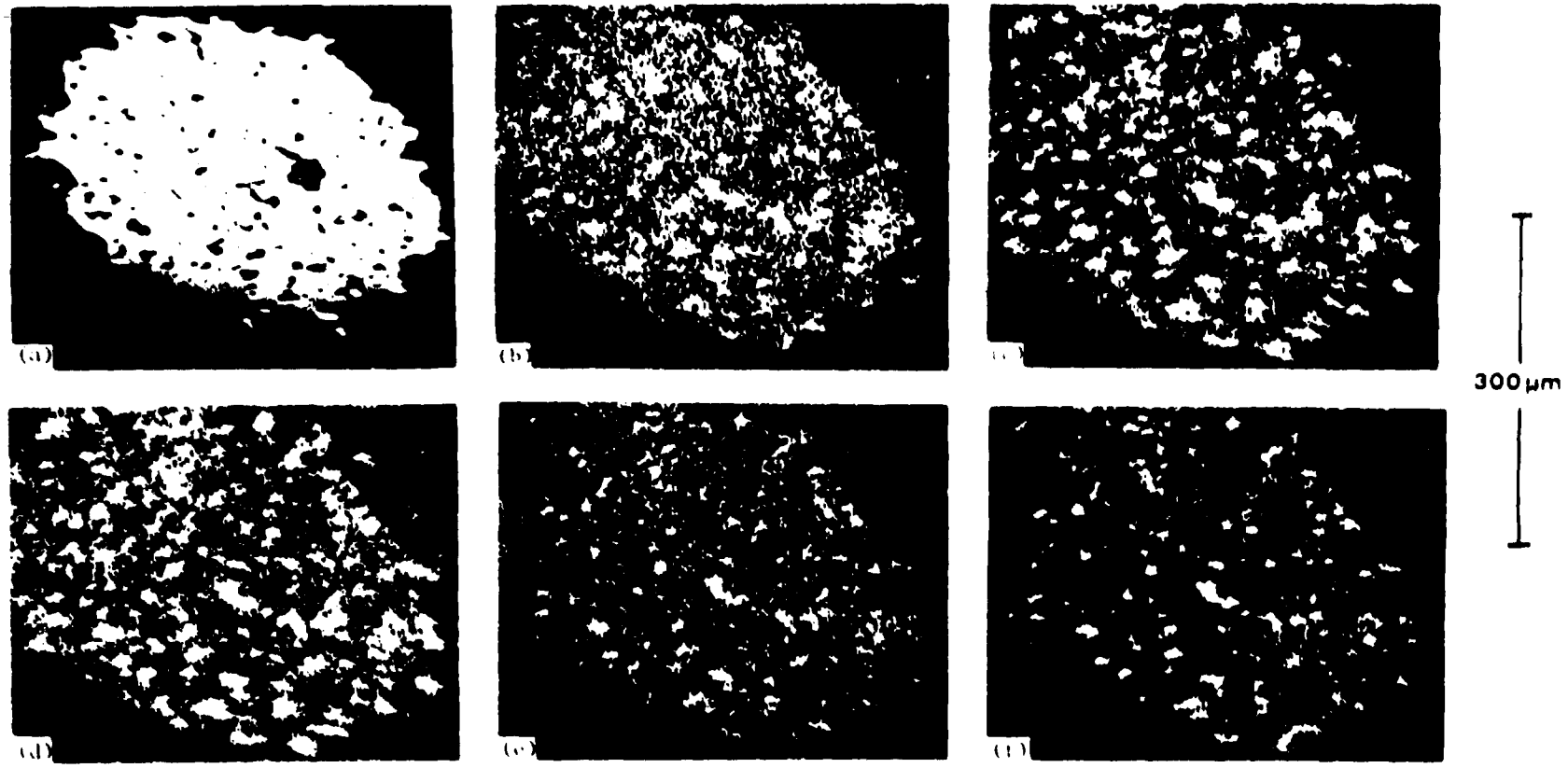

Fig. 14. Electron Microprobe Displays of Kernel of Biso-Coated Sol-Gel Particle. Same orientation as in Fig. 12. (a) Backscattered electron image. (b) Pd Lα. (c) Mo Lα. (d) Ru Lα. (e) Rh Lα. (f) Tc Lα.

concern because of its adverse effect on SiC corrosion.[25,26] Interestingly, with these dense sol-gel kernels some palladium is present in the metallic inclusions, whereas in low-density WAR particles palladium is not readily apparent in the metallic inclusions (of particles with conversions <15%).[25,26] Obviously, some of the palladium in the dense kernel's metallic inclusions is attributable to the decay of ^{106}Ru into stable ^{106}Pd. Also, some contribution to the Pd L_α x-ray display is caused by interference from the Ru L_β x-ray. Selective microprobe analysis did show palladium in the inclusions.

5.6.2 Triso-Coated Sol-Gel Particles

A metallographic cross-section through a Triso-coated sol-gel particle is shown in Fig. 15. As with the Biso-coated particles, the Triso-coated particles appeared to be in good condition with no broken SiC coatings. The outer LTI coating on some of the particles was probably broken, because of the high anisotropy of the coating.[27] This is most easily seen under polarized light illumination [Fig. 15(b)] as high optical activity. No outer layer of zirconium was observed with these particles. However, close examination of the SiC coating revealed small bright inclusions at the interface between SiC and the inner LTI and in the SiC [Fig. 15(c)].

The shielded electron microprobe identified these inclusions as palladium (Fig. 16). Evidently the palladium was free to migrate out of the Biso-coated particles, while in the Triso-coated particle the SiC coating slowed further migration. This penetration into the SiC coating is of major concern when dealing with LEU fuel particles because of the increased production of fission product palladium from ^{239}Pu fissions.

Examination of the kernel showed the actinides and the fission products to be distributed identically to the Biso-coated particle just discussed (Figs. 17, 18, and 19). Again, some of the palladium appears to be tied up in the metallic inclusions.

Cesium (not pictured) was located in the buffer and inner LTI coatings. The SiC coating appeared to provide an adequate barrier.

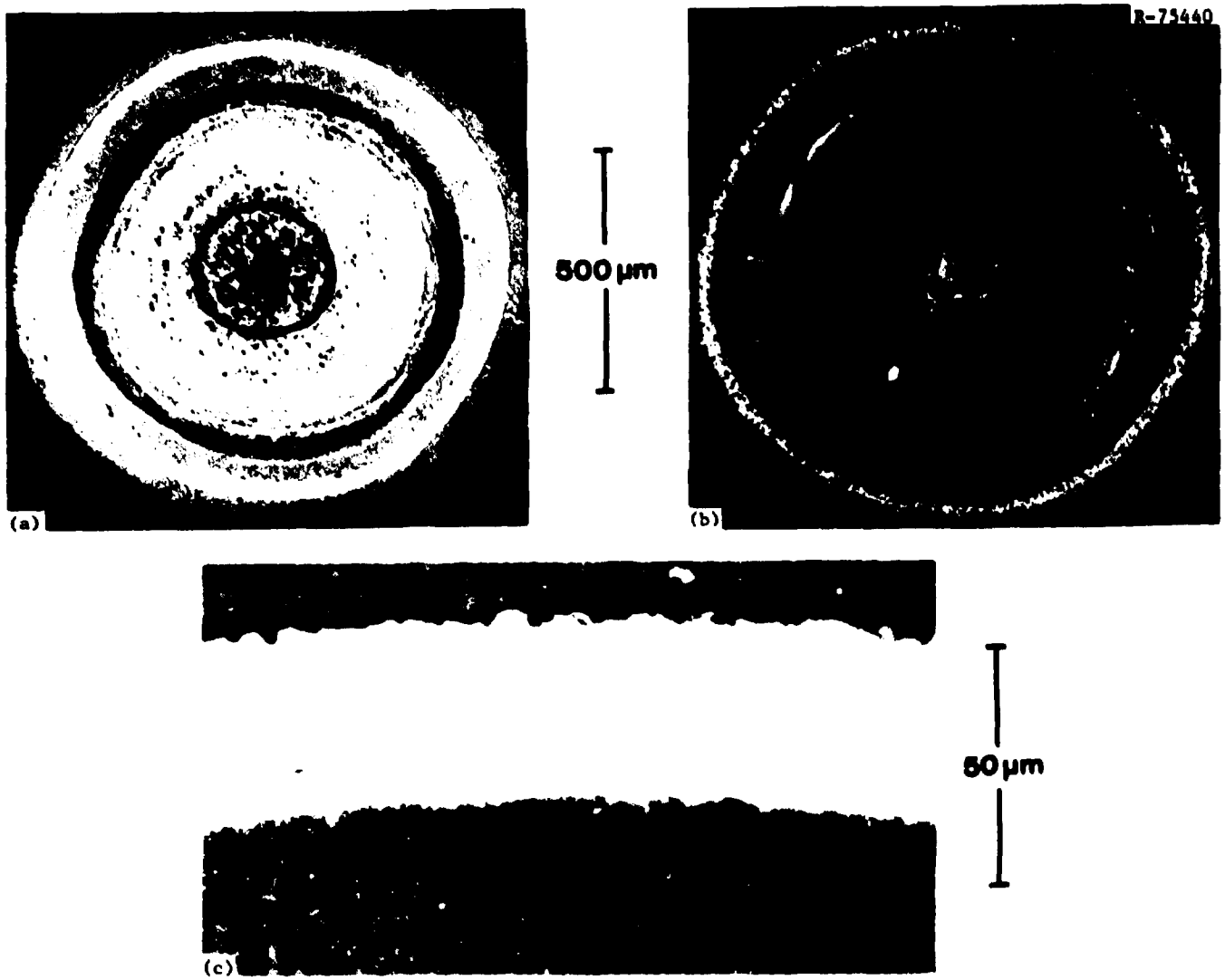

Fig. 15. Triso-coated sol-gel particle. (a) Bright field. (b) Polarized light. (c) High magnification of SiC coating.

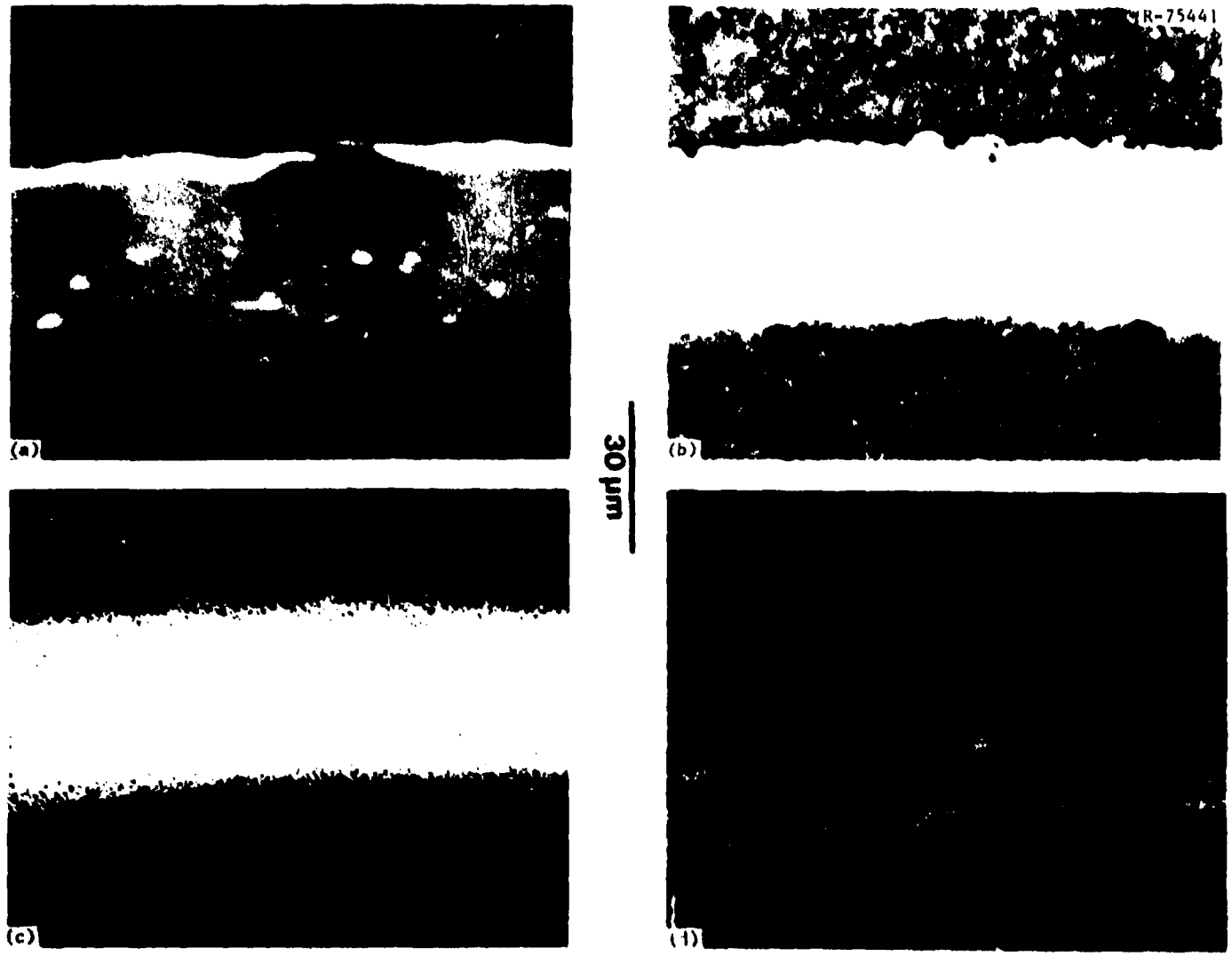

Fig. 16. Metallic Inclusions in SiC Identified as Palladium. (a) Backscattered electron image. (b) Optical, bright field. (c) Si Lα x-ray display. (d) Pd Lα x-ray display.

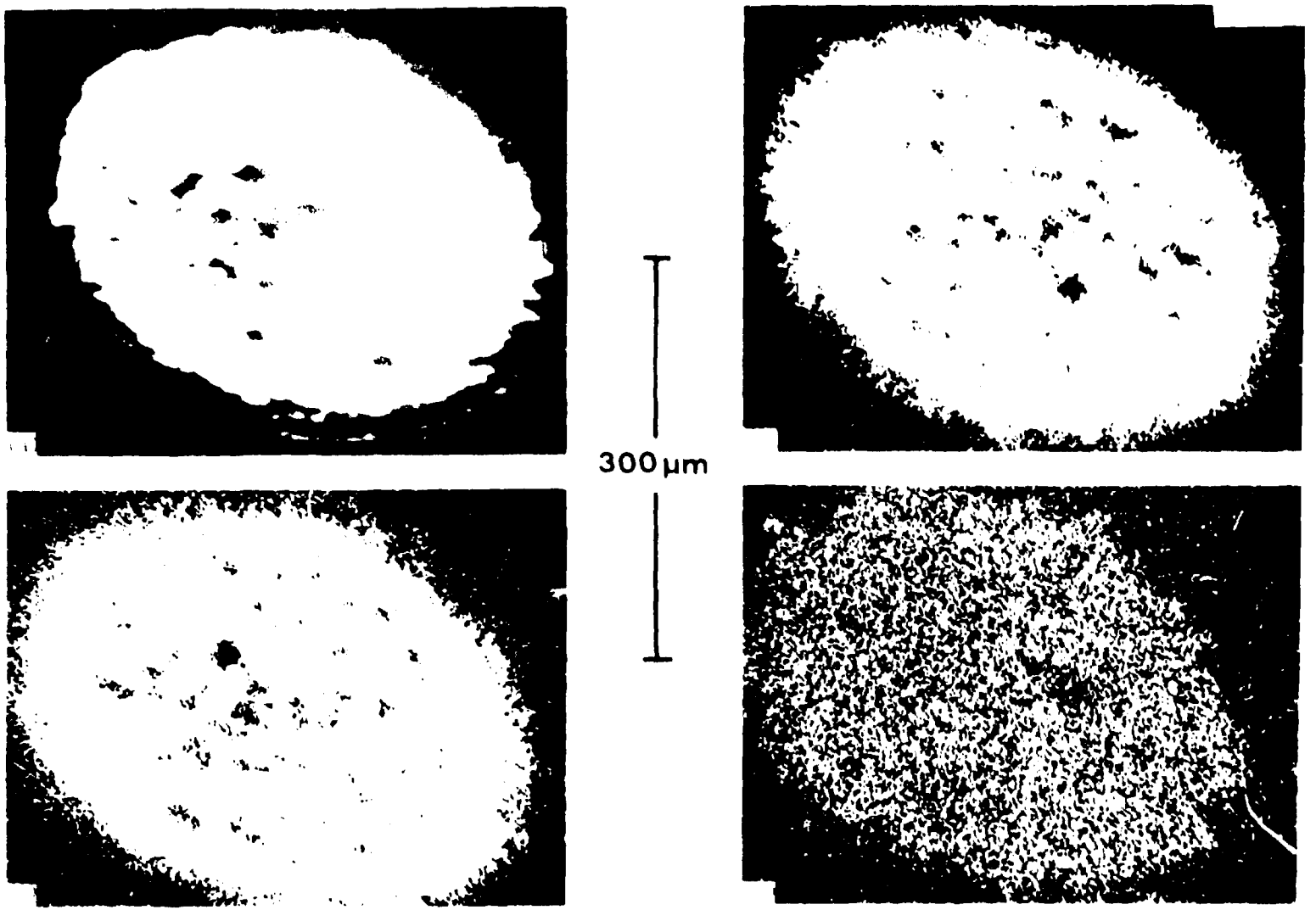

Fig. 17. Electron Microprobe Displays of Kernel of Triso-Coated Sol-Gel Particle. (a) Backscattered electron image. (b) U M$_\alpha$. (c) Pu M$_\alpha$. (d) Nd L$_\alpha$.

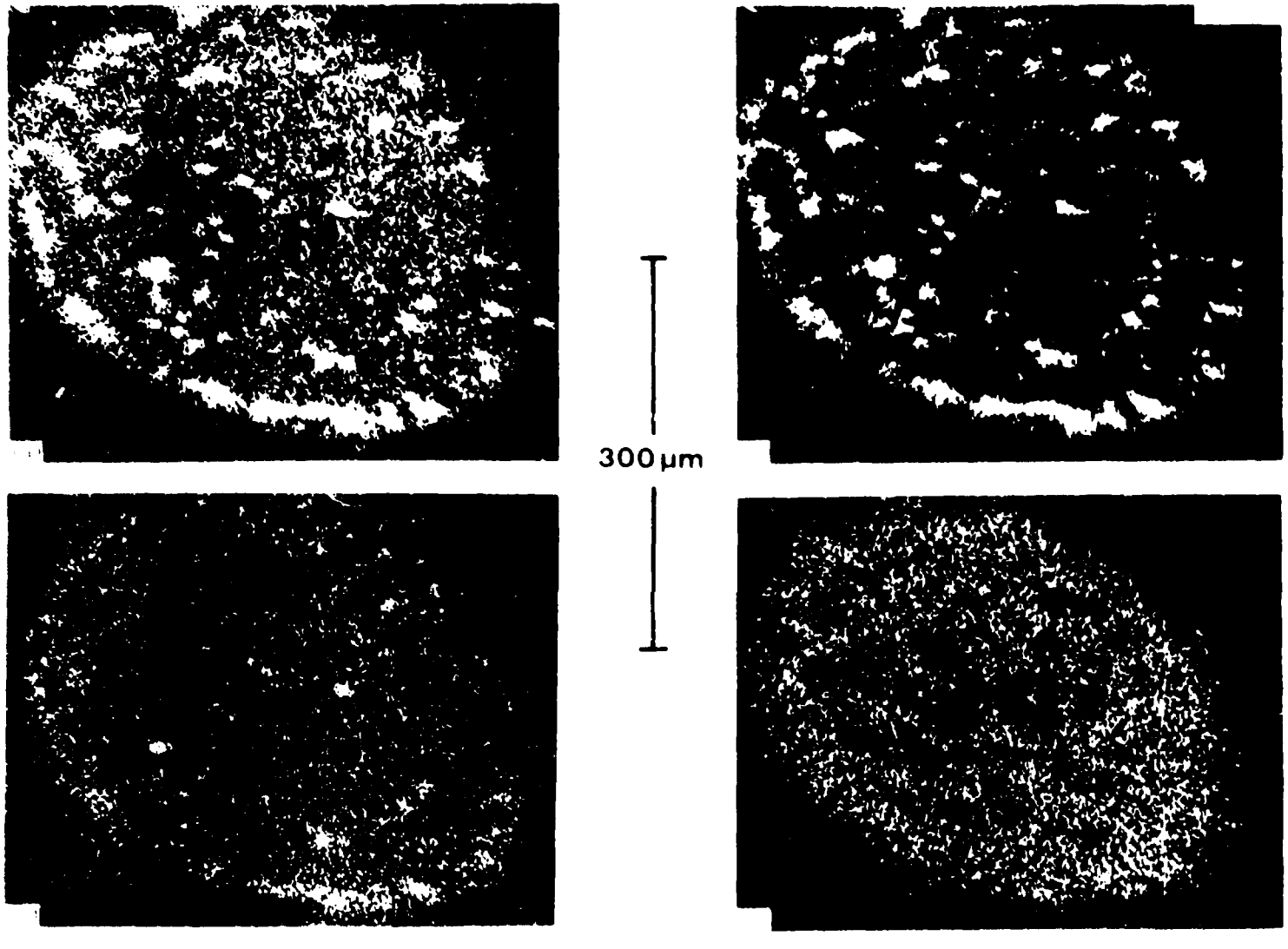

Fig. 18. Electron Microprobe X-ray Displays of Kernel of Irradiated [illegible]. [illegible] orientation as in Fig. 17. (a) Ce Lα. (b) Ba Lα. (c) Sr Lα. [illegible]

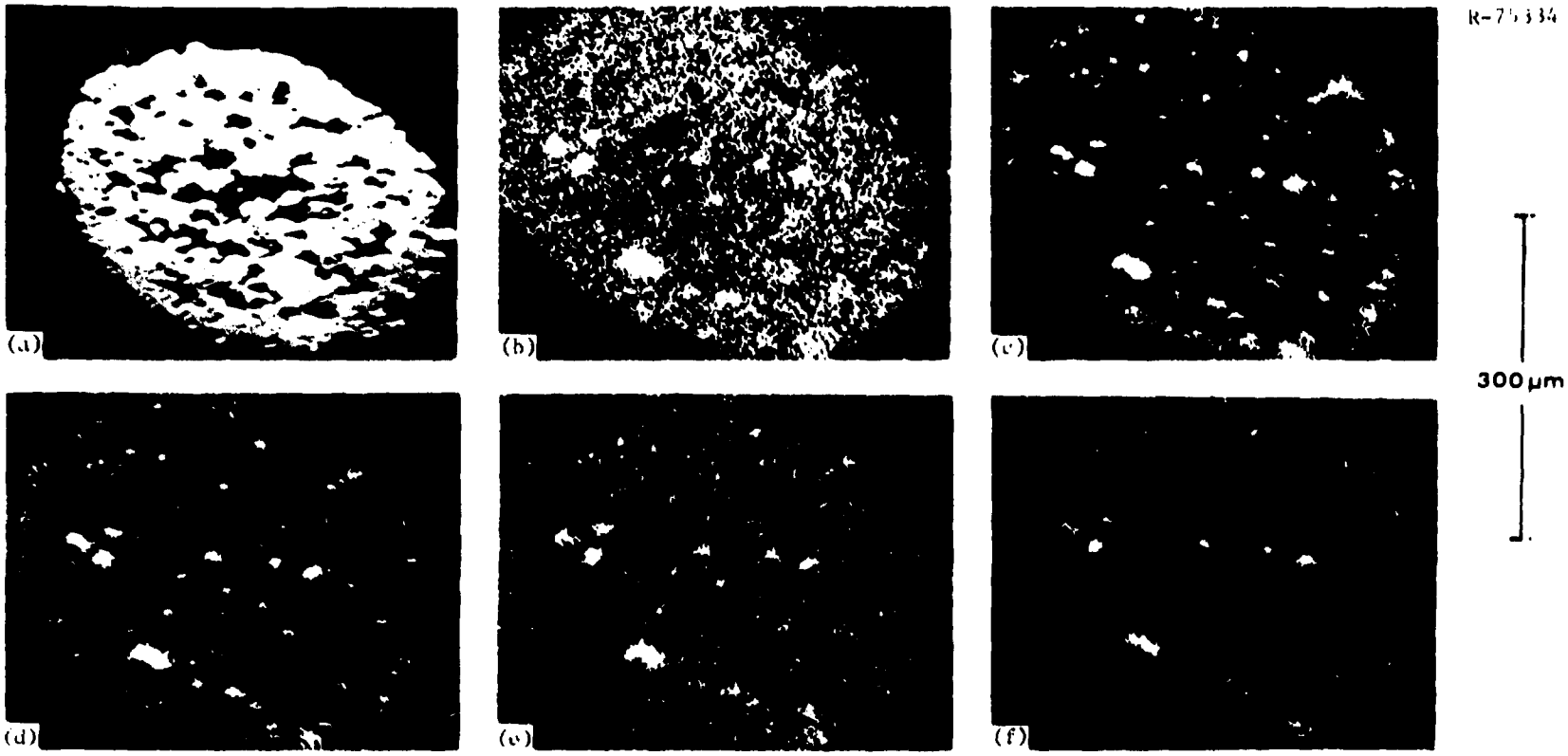

Fig. 19. Electron Microprobe Displays of Kernel of Triso-Coated Sol-Gel Particle. Same orientation as in Fig. 17. (a) Backscattered electron image. (b) Pd Lα. (c) Mo Lα. (d) Ru Lα. (e) Rh Lα. (f) Tc Lα.

5.7 Gamma Analysis of Normal UO_2 Particles

The individual normal UO_2 particles were scanned by the Irradiated Microsphere Gamma Analyzer system[28] before their metallographic examination. The complete results are presented in Appendix A. The quantitative analyses have been corrected for absorbtion by the coatings, and the activities have been calculated back to the date the capsule was removed from the reactor. Table 16 compares various fission products with one another. These comparisons can be used to determine the behavior of volatile and immobile fission products, such as cesium and zirconium, respectively.

The ratios of the ^{137}Cs to ^{95}Zr indicate that some cesium was lost from two Biso-coated particles during irradiation (contained in U-16) as compared with the Triso-coated particles (in U-17). Similar behavior has been observed in other Biso-coated fissile fuel and is the reason

Table 16. Comparisons of Selected Product Gamma Activities[a] With Each Other from the Norman UO_2 Particles

Sample	$^{134}Cs/^{137}Cs$	$^{137}Cs/^{95}Zr$	$^{110m}Ag/^{95}Zr$[b]	$^{144}Ce/^{95}Zr$
U-16-1	1.791	0.014		0.258
-2	1.831	0.014		0.273
-3	1.764	0.010		0.270
-4	1.797	0.012		0.273
av	1.796	0.013		0.269
U-17-1	1.819	0.014		0.273
-2	1.722	0.015	0.002	0.276
-3	1.802	0.015	0.002	0.279
-4	1.834	0.014		0.281
-5	1.860	0.014	0.002	0.269
av	1.807	0.014		0.275

[a]The ratios were calculated by use of all the gamma peaks detected for each isotope except ^{110m}Ag, where just the 884-keV peak was used.

[b]Ratio calculated only when ^{110m}Ag was detected.

why all fissile particles are now Triso-coated.[29,30] The cesium loss may be related to the permeability of the Biso-coated particles (Sect. 5.4).

The $^{134}Cs/^{137}Cs$ ratios are practically identical for both the Biso- and Triso-coated particles. We had hoped that the ratio could be used to indicate pyrocarbon permeability by inert gas fission products.[31] This is because ^{134}Cs is an activation product of ^{133}Cs, which has 5.27-d ^{133}Xe as its precursor. Ideally, with permeable pyrocarbon coatings the ^{133}Xe would be able to escape from the particle faster than the ^{137}Cs and the final result would be low $^{134}Cs/^{137}Cs$ ratios. Internal gas pressure measurements (Sect. 5.4) had shown that Biso-coated particles were permeable compared with the Triso-coated particles; however, no real differences in the $^{134}Cs/^{137}Cs$ ratios are observed. These preliminary results indicate that the time required for ^{133}Xe release, particularly from the kernel, is significantly longer than 5 d (i.e., the half-life of ^{133}Xe). Thus it seems that, at least for dense kernels, interpretation of the $^{134}Cs/^{137}Cs$ ratio may be difficult. Indications are that the $^{134}Cs/^{137}Cs$ ratio is still a good measure of performance of low-density fissile particles made from weak-acid resins.[31]

Cerium migration and subsequent SiC corrosion is of concern in HTGR fuel particles. The present results of the $^{144}Ce/^{95}Zr$ ratio in both the Biso- and Triso-coated particles confirm what was observed by the electron microprobe; that is, all the cerium is retained in the kernel. Similar results have been observed previously with UO_2 containing highly enriched uranium.[20]

An interesting observation was the presence of ^{110m}Ag in three of the five Triso-coated particles. (None was detected in any of the Biso-coated particles.) Silver is extremely volatile at the irradiation temperatures in these particles and is the major contributor to the radioactivity of the primary circulator in an HTGR. Thus its behavior is important especially when dealing with an LEU cycle for the HTGR because of the enhanced production of silver from plutonium fissions. Previous results[32] have hypothesized that silver can diffuse through pyrocarbon and SiC and escape from the particle. Studies are now under way to correlate SiC properties

with fission product release.[33] In any event, the presence of ^{110m}Ag in some Triso-coated particles indicates that the SiC provides some barrier, but retention is variable.

6. CONCLUSIONS

Irradiation capsule HT-31 was successful from the standpoint that original objectives were met. It furnished (1) irradiated inert fuel rods for thermal conductivity experiments, (2) irradiated natural UO_2 particles for internal gas pressure measurements, and (3) irradiated inert particles for pyrocarbon permeability studies besides irradiating material for GA and LASL.

The results on the thermal conductivity experiments were combined with other results and reported elsewhere.[7] Unexpectedly, the internal gas pressure measurements showed that oxygen release from plutonium fissions was less than calculated. The discrepancy may be due to a change in the O/U ratio as a result of the known solid solution of SrO and the rare earth oxides in UO_2. The permeability studies, although tentative, indicate that the pyrocarbon permeability decreases with increasing fast neutron fluence. While these objectives (coupled with GA's and LASL's) were the justification for the test, the additional work on LEU fuel tests may prove to be the most important results in the long run.

These additional tests were a direct result of the recent interest in using low-enriched uranium (LEU) in the fuel particles. Examination of sol-gel UO_2 particles (0.7% ^{235}U) with both Biso- and Triso-coatings revealed that most of the fission products (i.e., Nd, La, Pr, Ba, Zr, Sr, Cs, Mo, Ru, Rh, Tc) behaved similarly to those in particles containing 93%-enriched uranium. Thus, much of the data base that has been developed for the HEU fuel cycle can be applied to the LEU particles. Of interest with the LEU particles was the behavior of palladium and silver because of their enhanced production in LEU fuel due to ^{239}Pu fissions. Palladium penetrated into the SiC layer on Triso-coated particles. Silver, on the other hand, was not observed in the particles when examined with the electron microprobe. But gamma analysis showed that some retention of

^{110m}Ag (activation product of fission product ^{109}Ag) was provided by the Triso-coated particles, although it was variable. No ^{110m}Ag retention was observed with the Biso-coated particles.

The results also showed that Triso-coated particles should not be irradiated above approximately 1200°C without the outer pyrocarbon coating because the SiC coating degrades.

7. ACKNOWLEDGMENTS

The authors wish to acknowledge the efforts of many people who made significant contributions to the planning, execution, and interpretation of this experiment. First, we wish to thank F. J. Homan and W. P. Eatherly for their many efforts in planning this capsule and for guidance and direction throughout the total effort. Also acknowledged is the assistance of J. A. Conlin, K. R. Thoms, and B. H. Montgomery, who participated in the planning, design, construction, and irradiation of the capsule. G. W. Weber, C. Hamby, and J. F. Willmering assisted in producing the pyrolytic carbon coatings on the test particles, and the silicon carbide coatings were supplied by J. I. Federer and J. W. Geer. R. L. Hammer, D. E. Rosson, and H. Keating fabricated and characterized specimens, and M. D. Allen, W. J. Mason, L. G. Shrader, and E. R. Boyd performed metallography and radiography. The capsule was disassembled by E. L. Ryan and the staff of the High Radiation Level Examination Laboratory. Gas permeability and gamma spectroscopy were measured by G. L. Powell and G. A. Moore, respectively, and postirradiation microprobe work was done by T. J. Henson. The authors also wish to thank R. J. Lauf and G. W. Weber for their critical review and most helpful comments. Finally, we wish to acknowledge the efforts of those who helped in the preparation of this report — S. Peterson for technical editing and Shirley Frykman for word processing and makeup.

8. REFERENCES

1. W. J. Kovacs, C. A. Young, and D. P. Harmon, *Preirradiation Report of TRISO and BISO Coated ThO_2 Particles for Irradiation in Capsules HT-31 and HT-33,* GA-A-13923 (November 1976).

2. P. Wagner et al., *Irradiation Test HT-31: High-Temperature Irradiation Behavior of LASL-Made Extruded Fuel Rods and LASL-Made Coated Particles,* LA-6785-MS (April 1977).

3. E. L. Long, Jr., P. Krautwasser, R. L. Beatty, M. J. Kania, C. S. Morgan, R. L. Hamner, and C. S. Yust, *Characterization Studies and Performance of Biso-Coated Fertile Particles Irradiated in Capsules HT-28 Through HT-30,* (report in preparation).

4. J. P. Moore and T. G. Godfrey, "Capsules HT-20 Through -23," *HTGR Base-Technology Program Prog. Rep. July 1, 1975–Dec. 31, 1976,* ORNL-5274, pp. 221–26.

5. M. J. Kania, *HTCAP-A FORTRAN IV Program for Calculating Coated-Particle Operating Temperatures in HFIR Target Irradiation Experiments,* ORNL/TM-5332 (May 1976).

6. "Capsules HT-31 and HT-33," *HTGR Fuels and Core Development Quart. Prog. Rep. Feb. 28, 1977,* GA-A14298, pp. 9-38–9-42.

7. J. P. Moore, T. G. Godfrey, R. S. Graves, F. J. Weaver, W. P. Eatherly, and E. L. Long, Jr., *Experimental Determinations of the Pre- and Post-irradiation Thermal Transport and Thermal Expansion Properties of Simulated Fuel Rods for an HTGR,* ORNL-5414 (July 1978).

8. C. S. Morgan and G. L. Powell, "Inert Gas Intrusion as a Characterization Procedure for Pyrocarbon Coatings," (Summary) *Trans. Am. Nucl. Soc.* 28: 182–83 (June 1978).

9. M. J. Kania, T. B. Lindemer, M. T. Morgan, and J M Robbins, *Irradiation Performance of HTGR Fertile Fuel in HFIR Target Capsules HT-12 through HT-15: Part I – Experiment Description and Fission Product Behavior,* ORNL/TM-5305 (February 1977).

10. T. B. Lindemer, "Measurement and Interpretation of CO and Kr + Xe in Irradiated ThO_2 Containing HTGR Fuel Particles," *J. Am. Ceram. Soc.,* 60: 409–16 (1977).

11. R. H. Flowers and G. W. Horsley, *The Influence of Oxide Kernels on the Manufacture and Performance of Coated Particle Fuel,* AERE-R-5949 (1968).

12. G. W. Horsley et al., "Influence of Irradiation Temperature, Burnup and Fuel Composition on Gas Pressure (Xe, Kr, CO, CO_2) in Coated Particle Fuels," *J. Am. Ceram. Soc.* 59: 1–4 (1976).

13. T. B. Lindemer and H. J. de Nordwall, *An Analysis of Chemical Failure of Coated UO_2 and Other Oxide Fuels in the High-Temperature Gas-Cooled Reactor*, ORNL-4926 (1974).

14. P. E. Potter, "Some Phase Equilibria and Thermodynamic Considerations for Irradiated Oxide Nuclear Fuels," pp 115–55 in *Behavior and Chemical State of Irradiated Ceramic Fuels*, International Atomic Energy Agency, Vienna, 1974.

15. J. Drowart, G. DeMaria, and M. G. Ingraham, "Thermodynamic Study of SiC Utilizing a Mass Spectrometer," *J. Chem. Phys.* 29: 1015–21 (1958).

16. P. Grieveson and C. B. Alcock, "The Thermodynamics of Metal Silicides and Silicon Carbide," p. 183 in *Special Ceramics*, P. Popper, ed., Academic Press, Inc., New York, 1960.

17. R. J. Price, "Properties of Silicon Carbide for Nuclear Fuel Particle Coatings," *Nucl. Technol.* 35(2): 320–36 (September 1977).

18. R. L. Hamner, "Capsule HT-33," *HTGR Base-Technology Program Prog. Rep., July 1, 1975–Dec. 31, 1976*, ORNL-5274, pp. 257–70.

19. T. N. Tiegs, A. J. Caputo, E. L. Long, Jr., and B. H. Montgomery, *Irradiation Performance of HTGR Fuel Rods in HFIR Experiments HT-26 and -27*, ORNL/TM-5404 (August 1976).

20. K. H. Valentine, F. J. Homan, E. L. Long, Jr., T. N. Tiegs, B. H. Montgomery, R. L. Hamner, and R. L. Beatty, *Irradiation Performance of HTGR Fuel Rods in HFIR Experiments HRB-7 and -8*, ORNL-5228 (May 1977).

21. T. N. Tiegs and T. J. Henson, *Fission Product Behavior in HTGR Fuel Particles Made from Weak-Acid Resins*, (report in preparation).

22. D. R. O'Boyle, F. L. Brown, and J. E. Sanecki, "Solid Fission Product Behavior in Uranium-Plutonium Oxide Fuel Irradiated in a Fast Neutron Flux," *J. Nucl. Mater.* 29: 27–42 (1969).

23. C. A. Friskney and K. A. Simpson, "The Behavior of Fission Product Barium and Strontium in Irradiated UO_2," *J. Nucl. Mater.* 57: 121–22 (1975).

24. H. Kleykamp, *Microprobe Study of Fission Product Behavior in High-Burnup HTR-Fuels*, KFK-2213 (Sept. 1, 1975).

25. T. N. Tiegs and K. R. Thoms, *Operation and Postirradiation Examination of ORR Capsule OF-2: Accelerated Testing of HTGR Fuel*, ORNL-5428 (in press).

26. T. N. Tiegs et al, *Irradiation Performance of HTGR Fuel in HFIR Capsule HT-33*, (report in preparation).

27. T. N. Tiegs, E. L. Long, Jr., M. J. Kania, K. R. Thoms, and E. J. Allen, *ORR Irradiation Experiments OF-1: Accelerated Testing of HTGR Fuel*, ORNL-5324 (August 1977).

28. K. H. Valentine and E. L. Long, Jr., "Fuel Particle Inspection with an Irradiated Microsphere Gamma Analyzer," *Trans. Am. Nucl. Soc.* 22: 213–14 (November 1975).

29. F. J. Homan and E. L. Long, Jr., *Irradiation Performance of HTGR Recycle Fissile Fuel*, ORNL/TM-5502 (August 1976).

30. T. N. Tiegs and E. L. Long, Jr., *Postirradiation Examination of Recycle Test Elements from the Peach Bottom Reactor*, ORNL-5422 (December 1978).

31. Personal communication, M. J. Kania, Oak Ridge National Laboratory, May 1978.

32. H. Nabielek, P. E. Brown, and P. Offermann, "Silver Release from Coated Particle Fuel," *Nucl. Technol.* 35(2): 483–93 (September 1977).

33. Personal communication, G. W. Weber, Oak Ridge National Laboratory, May 1978.

APPENDIX

Analysis of Gamma Spectra from Individual Fuel Particles Irradiated in Positions U-16 and U-17 of HT-31

APPENDIX

Analysis of Gamma Spectra from Individual Fuel Particles Irradiated in Positions U-16 and U-17 of HT-31

The analysis for each particle is presented as a printout in the pages that follow. The top of each printout gives the date and time (24-h) that the gamma spectrum was acquired and the identification of the spectrum.

The meanings of the column headings in the printouts are as follows:

F. P. — The chemical symbol and isotope number of all emitters in the isotope table that are identified with the peak.* Isotopes listed without any peak number are really contributors to preceeding peak.

ENERGY (KEV) — The energy (in keV) that corresponds to the peak centroid.

PEAK CHNL — The channel number of the peak centroid (not the channel containing the peak number of counts, as the name would imply).

CPS — The rate, in counts/s, at which all characteristic gamma rays having the centroid energy are detected.

GAMMA/SEC — The rate at which characteristic gamma rays at the centroid energy are emitted by the source.

ERR (%) — This number is an estimate of the statistical uncertainty (due to the random nature of the radioactive decay process) that should be associated with the measurement of CPS (and therefore with GAMMA/SEC as well). The best interpretation is to assume that the probability is 68% that the true value of CPS deviates from the listed value by less than the listed error.

BW — The number of histogram channels involved in the calculation of CPS.

MU — The order of the multiplet of which the listed peak is a member. This number includes all local maxima that were detected in the base width even though some of them may not have satisfied the necessary criteria for being listed as a separate peak.

---

*The following exceptions apply to the printed identification of the fission products: (1) the unknown at 74 keV and the ^{233}Pa at 85 keV are really fluorescent x rays from Pb; (2) the ^{233}Pa peaks at 94, 98, and 114 keV and the ^{125}Te at 111 keV are really fluorescent x rays from U.

FWHM (KEV) The peak's full width at half maximum (in keV). This number is useful for spotting unresolved multiplets, which often have abnormally high FWHMs. If it is not possible for the program to calculate the FWHM (which, for example, sometimes occurs for the central peak of a triplet), a zero will be printed in this column.

PK # A sequential number assigned to each peak.

HI-21, U-16, PHOTOFILE #1

F P	ENERGY (KEV)	PEAK CHNL	CPS	GAMMA/SEC	ERR (%)	BW	MU	FWHM (KEV)	PK #
???	74 10	104 76	44 28	2 01bE+06	1 27	48	5	89	1
CE144	79 94	112 15	14b 81	5 500E+05	2 60	48	5	2 41	2
PA233	85 26	120 80	200 71	b 570E+05	2 02	48	5	3 34	3
EU155									
PA233	94 81	134 51	152 68	4 208E+05	2 51	48	5	2 95	4
PA233	98 12	139 56	257 41	b 822E+05	1 73	48	5	2 64	5
TE125	111 11	157 92	75 741	1 819E+05	4 91	16	2	3 58	6
PA233									
PA233	114 94	162 86	10 168	2 146E+04	8 86	16	2	1 29	7
EU154	122 98	174 99	19 517	b 099E+04	11 29	5	1	1 83	8
CE144	133 47	190 05	1bb7 3	2 983E+06	0 67	19	1	2 37	9
SB125	427 82	612 87	19 165	1 192E+05	11 02	7	1	2 21	10
RU106	511 89	733 61	1029 8	7 811E+06	0 45	16	1	2 56	11
CS134	563 33	807 49	59 795	4 978E+05	3 74	24	2	2 77	12
CS134	569 45	816 29	118 74	9 997E+05	2 59	24	2	2 63	13
CS134	604 79	867 02	666 11	5 967E+05	0 bb	17	1	2 49	14
RU106	616 26	884 50	28 335	2 587E+05	5 15	20	2	2 10	15
RU106	622 12	891 92	411 48	3 794E+06	0 81	20	2	2 55	16
CS137	661 68	948 72	458 62	4 501E+06	0 70	16	1	2 60	17
CE144	696 65	998 94	38 118	3 939E+05	3 99	9	1	2 51	18
ZR95	724 21	1038 52	68 010	7 302E+05	2 70	12	1	2 70	19
EU154									
ZR95	756 85	1085 38	71 982	8 072E+05	2 14	27	3	2 69	20
EU154									
NB95	765 69	1098 08	282 77	3 207E+06	1 00	27	3	2 37	21
AG110M									
CS134	795 93	1141 49	449 34	5 292E+06	0 65	23	2	2 76	22
CS134	802 04	1150 27	50 485	5 991E+05	2 56	23	2	2 75	23
RU106	873 56	1252 96	15 036	1 937E+05	7 19	9	1	2 39	24
EU154									
EU154	1004 00	1440 24	2 1114	3 102E+04	18 69	7	2	1 25	25
EU154	1005 24	1442 01	2 9898	4 398E+04	14 10	7	2	1 63	26
RU106	1050 51	1507 01	34 656	5 313E+05	2 97	11	1	2 67	27
EU154	1128 16	1618 47	9 0300	1 479E+05	7 74	9	1	2 54	28
RU106									
CS134	1168 14	1675 86	3 5150	5 947E+04	18 45	9	1	2 26	29
EU154	1274 50	1828 72	9 5450	1 752E+05	5 86	9	1	2 63	30
CS134	1365 20	1958 70	9 5975	1 878E+05	5 55	11	1	2 67	31
???	1407 30	2019 14	1 9025	3 630E+04	17 13	6	1	1 69	32
CE144	1489 29	2136 80	3 1112	6 611E+04	9 94	7	1	2 41	33
???	1561 98	2241 11	2 1825	4 853E+04	13 61	9	1	2 50	34
???	1988 86	2852 59	27500	7 751E+03	38 62	5	1	1 40	35
CE144	2185 77	3136 05	6 5912	2 047E+05	4 60	17	1	3 71	36
???	2405 18	3450 72	70000	1 031E+04	24 15	10	1	1 57	37

11 -16 -1977 1358 29

HT-31. U-16. PARTICLE #2

F P	ENERGY (KEV)	PEAK CHNL	CPS	GAMMA/SEC	EFF (%)	BW	MU	FWHM (KEV)	PK #
???	74.28	105.02	433.29	1.946E+06	1.38	54	6	3.83	1
CE144	80.13	113.43	148.60	5.502E+05	2.68	54	6	2.76	2
PA233	85.06	120.50	200.04	6.538E+05	2.11	54	6	2.22	3
EU155									
PA233	94.52	134.09	152.76	4.218E+05	2.59	54	6	2.25	4
PA233	98.36	139.61	258.79	6.814E+05	1.82	54	6	2.50	5
TE125	111.21	158.08	88.820	2.120E+05	6.21	16	1	2.97	6
PA233									
CE144	133.54	190.15	940.62	2.768E+06	0.62	15	1	2.37	7
SB125	428.00	613.13	21.995	1.361E+05	9.49	7	1	2.95	8
CS134	475.86	681.87	16.590	1.149E+05	12.51	8	1	2.19	9
KR85	512.15	733.98	970.30	7.267E+06	0.46	15	1	2.55	10
RU106									
CS134	563.57	807.84	55.044	4.557E+05	3.68	19	2	2.71	11
CS134	569.60	816.50	99.234	8.206E+05	2.56	19	2	2.58	12
CS134	605.06	867.42	624.87	5.566E+06	0.61	16	1	2.74	13
SB125									
RU106	616.47	883.80	23.487	2.132E+05	6.48	22	2	2.78	14
RU106	622.42	892.34	381.60	3.499E+06	0.92	22	2	2.65	15
CS137	662.07	949.28	416.69	4.067E+06	0.74	15	1	2.62	16
CE144	696.90	999.30	34.332	3.527E+05	4.73	10	1	2.70	17
ZR95	724.43	1038.83	59.960	6.402E+05	2.84	11	1	2.76	18
EU154									
ZR95	756.69	1085.15	63.430	7.069E+05	2.50	33	3	1.99	19
EU154									
NB95	766.29	1098.94	262.57	2.962E+06	1.23	33	3	3.00	20
CS134	796.15	1141.81	425.90	4.987E+06	0.73	27	2	2.74	21
CS134	802.20	1150.50	49.586	5.850E+05	2.65	27	2	3.30	22
RU106	873.99	1253.58	12.585	1.612E+05	10.88	13	1	2.39	23
EU154									
EU154	1005.53	1442.43	4.3500	6.362E+04	16.62	8	1	2.86	24
RU106	1050.85	1507.49	32.917	5.017E+05	3.09	11	1	2.93	25
EU154	1128.60	1619.11	6.2337	1.031E+05	10.62	9	1	3.01	26
RU106									
EU154	1274.97	1829.20	7.6725	1.400E+05	6.95	9	1	2.63	27
???	1333.48	1913.18	1.5475	2.945E+04	28.59	10	2	1.80	28
CS134	1365.46	1959.08	7.6200	1.483E+05	5.97	8	1	3.36	29
???	1408.26	2020.51	3.5937	7.200E+04	10.98	9	1	3.47	30
CE144	1489.66	2137.33	2.0512	4.333E+04	12.32	5	1	1.39	31
???	1563.41	2243.16	2.2100	4.888E+04	12.47	8	1	2.93	32
???	1927.40	2765.42	.40500	1.099E+04	28.58	5	1	1.27	33
CE144	2186.49	3137.08	5.9925	1.850E+05	4.82	14	1	3.33	34

11 -16 -1977 1403.31

HT-31, U-16, PARTICLE #3; 30 CM GEOMETRY (ALSO FOR #1 AND #2).

F. P.	ENERGY (KEV)	PEAK CHNL	CPS	GAMMA/SEC	ERR (%)	BW	MU	FWHM (KEV)	PK #
???	74.92	105.94	462.56	2.000E+06	1.31	36	4	5.29	1
CE144	80.40	113.82	157.71	5.630E+05	2.58	36	4	3.08	2
PA233	84.76	120.07	206.00	6.585E+05	2.14	36	4	2.15	3
EU155									
PA233	94.85	134.58	117.69	3.142E+05	2.59	16	2	2.49	4
PA233	98.53	139.85	200.19	5.111E+05	1.84	16	2	2.41	5
TE125	111.11	157.94	68.715	1.594E+05	5.05	9	1	2.46	6
PA233									
CE144	133.56	190.18	992.22	2.836E+06	0.63	18	1	2.32	7
SB125	176.62	252.03	9.1750	2.585E+04	26.82	7	1	1.75	8
SB125	428.40	613.69	19.975	1.201E+05	9.60	7	1	2.13	9
I'R85	512.12	733.94	1028.5	7.482E+06	0.43	16	1	2.43	10
RU106									
CS134	563.58	807.85	44.786	3.601E+05	4.40	22	2	2.34	11
CS134	569.58	816.46	77.998	6.342E+05	3.18	22	2	2.72	12
CS134	605.00	867.33	439.02	3.798E+06	0.74	15	1	2.46	13
SB125									
RU106	616.54	883.90	28.990	2.557E+05	4.57	21	2	2.35	14
RU106	622.24	892.09	405.98	3.615E+06	0.78	21	2	2.58	15
CS137	661.90	9[illegible]9.03	311.91	2.956E+06	0.83	14	1	2.55	16
CE144	6[illegible]6.86	9[illegible]9.25	38.410	3.833E+05	4.32	12	1	2.52	17
ZR95	7[illegible]4.49	1038.91	65.665	6.811E+05	2.52	12	1	2.57	18
EU154									
ZR95	756.99	1085.58	69.582	7.536E+05	2.03	26	2	2.77	19
EU154									
NB95	766.06	1098.61	276.51	3.029E+06	0.94	26	2	2.65	20
CS134	796.09	1141.73	310.92	3.537E+06	0.77	21	2	2.65	21
CS134	802.16	1150.44	30.561	3.502E+05	3.42	21	2	2.86	22
RU106	873.63	1253.06	13.360	1.661E+05	6.58	8	1	2.26	23
EU154									
EU154	996.42	1429.35	1.6550	2.331E+04	31.39	6	1	2.00	24
RU106	1050.79	1507.40	37.955	5.619E+05	2.60	12	1	2.86	25
EU154	1128.49	1618.95	9.1750	1.452E+05	8.06	12	1	2.64	26
RU106									
EU154	1274.71	1828.84	9.3575	1.658E+05	5.92	11	1	2.72	27
???	1332.71	1912.07	1.9300	3.566E+04	18.21	8	1	2.98	28
CS134	1365.76	1959.51	6.2687	1.185E+05	6.69	9	1	2.33	29
???	1408.23	2020.46	3.6100	7.025E+04	9.26	8	1	2.72	30
CE144	1489.61	2137.25	3.4487	7.077E+04	9.16	9	1	2.19	31
???	1562.00	2241.25	1.3675	2.936E+04	16.82	6	1	1.40	32
CE144	2186.36	3136.89	7.0275	2.100E+05	4.38	14	1	3.00	33

11 -16 -1977 1505.53

HT-31, U-16, PARTICLE #4; 30 CM GEOMETRY.

F.P.	ENERGY (KEV)	PEAK CHNL	CPS	GAMMA/SEC	ERR (%)	BW	MU	FWHM (KEV)	PK #
???	74.29	105.03	399.58	1.767E+06	1.35	48	5	3.92	1
CE144	80.13	113.42	138.48	5.054E+05	2.71	48	5	2.71	2
PA233	85.06	120.51	178.33	5.743E+05	2.21	48	5	3.20	3
EU155									
PA233	94.53	134.11	140.66	3.827E+05	2.67	48	5	2.12	4
PA233	98.35	139.60	241.84	6.275E+05	1.82	48	5	2.53	5
TE125	111.37	158.30	95.032	2.233E+05	5.13	14	1	2.83	6
PA233									
CE144	133.53	190.14	924.70	2.681E+06	0.66	17	1	2.34	7
SB125	428.47	613.80	19.510	1.191E+05	9.25	6	1	1.51	8
KR85	512.14	733.97	951.98	7.025E+06	0.51	19	1	2.53	9
RU106									
CS134	562.61	807.89	46.016	3.754E+05	4.25	20	2	2.58	10
CS134	569.59	816.48	83.998	6.928E+05	2.96	20	2	2.72	11
CS134	605.06	867.42	523.86	4.598E+06	0.69	16	1	2.73	12
SB125									
RU106	616.57	883.95	26.097	2.335E+05	5.59	21	2	2.13	13
RU106	622.41	892.33	366.81	3.314E+06	0.89	21	2	2.65	14
CS137	662.06	949.27	354.00	3.404E+06	0.82	15	1	2.66	15
CE144	696.90	999.30	37.265	3.773E+05	4.17	10	1	2.82	16
ZR95	724.53	1038.97	58.575	6.163E+05	2.95	12	1	2.51	17
EU154									
ZR95	757.04	1085.66	64.443	7.080E+05	2.30	27	2	2.78	18
EU154									
NB95	766.11	1098.68	253.34	2.816E+06	1.07	27	2	2.78	19
CS134	796.13	1141.78	357.47	4.125E+06	0.74	22	2	2.76	20
CS134	802.50	1150.93	38.207	4.443E+05	3.13	22	2	2.63	21
RU106	873.68	1253.13	15.045	1.898E+05	7.19	10	1	2.44	22
EU154									
RU106	1050.83	1507.46	32.205	4.837E+05	3.33	13	1	2.84	23
EU154	1128.74	1619.30	8.6375	1.386E+05	7.36	9	1	2.89	24
RU106									
CS134	1168.54	1676.43	2.7612	4.578E+04	14.94	5	1	1.44	25
EU154	1275.12	1829.42	8.5950	1.546E+05	6.39	10	1	3.30	26
CS134	1365.79	1959.56	6.6950	1.284E+05	6.48	9	1	2.42	27
???	1562.75	2242.22	1.6312	3.554E+04	14.82	7	1	2.17	28
CE144	2186.41	3136.96	5.7675	1.754E+05	4.97	14	1	3.67	29

11 -16 -1977 1535.28

HT-31, U-17, PARTICLE #1; 30 CM GEOMETRY.

F.P.	ENERGY (KEV)	PEAK CHNL	CPS	GAMMA/SEC	ERR (%)	BW	MU	FWHM (KEV)	PK #
???	74.07	104.71	436.52	2.008E+06	1.32	49	5	3.90	1
CE144	79.90	113.10	148.87	5.639E+05	2.60	49	5	2.39	2
PA233	85.00	120.43	197.74	6.575E+05	2.08	49	5	3.05	3
EU155									
PA233	94.49	134.05	147.08	4.128E+05	2.60	49	5	2.22	4
PA233	98.30	139.53	235.74	6.310E+05	1.87	49	5	2.49	5
TE125	111.00	157.77	45.957	1.115E+05	8.59	10	1	2.45	6
PA233									
EU154	123.12	175.19	21.870	6.881E+04	14.31	8	1	2.71	7
CE144	133.46	190.04	1053.7	3.148E+06	0.54	14	1	2.37	8
SB125	428.02	613.15	26.478	1.662E+05	9.75	9	1	2.86	9
RU106	511.87	733.58	1071.2	8.136E+06	0.44	16	1	2.60	10
CS134	563.29	807.43	60.536	5.082E+05	3.45	20	2	2.47	11
CS134	569.45	816.27	119.48	1.014E+06	2.30	20	2	2.62	12
CS134	604.76	866.99	694.36	6.272E+06	0.56	15	1	2.56	13
RU106	616.34	883.62	26.901	2.477E+05	5.55	20	2	2.22	14
RU106	622.00	891.74	419.60	3.901E+06	0.81	20	2	2.57	15
CS137	661.82	948.93	469.04	4.643E+06	0.79	20	2	2.88	16
???	677.56	971.53	2.7212	2.758E+04	36.19	5	1	1.27	17
CE144	696.49	998.71	39.586	4.124E+05	4.47	11	1	2.51	18
ZR95	724.20	1038.49	64.720	7.008E+05	2.90	12	1	2.64	19
EU154									
ZR95	756.79	1085.30	74.107	8.380E+05	2.12	27	2	2.61	20
EU154									
NB95	765.87	1098.34	286.63	3.279E+06	1.01	27	2	2.73	21
AG110M									
CS134	795.90	1141.46	476.94	5.664E+06	0.61	21	2	2.76	22
CS134	801.79	1149.91	51.241	6.129E+05	2.55	21	2	3.14	23
RU106	873.41	1252.74	16.745	2.174E+05	7.01	10	1	2.63	24
EU154									
EU154	1004.65	1441.16	6.3975	9.484E+04	13.87	10	1	3.89	25
RU106	1050.35	1506.77	38.156	5.897E+05	2.79	11	1	2.79	26
EU154	1127.89	1618.09	9.8600	1.628E+05	10.82	16	2	1.98	27
RU106									
CS134	1167.74	1675.[illegible]	5.3912	9.196E+04	10.65	7	1	2.05	28
EU154	1274.54	1828.58	8.8625	1.640E+05	6.62	10	1	2.96	29
CS134	1365.18	1958.68	9.8525	1.944E+05	5.31	10	1	2.98	30
???	1408.15	2020.35	4.0000	8.289E+04	9.73	9	1	3.03	31
CE144	1489.16	2136.62	3.3900	7.261E+04	9.24	7	1	2.83	32
???	1561.94	2241.06	2.1825	4.892E+04	11.68	6	1	2.15	33
CE144	2185.55	3135.73	7.7937	2.439E+05	4.10	13	1	3.05	34

11 -16 -1977 1541 10

HT-31, U-17, PARTICLE #2; 30 CM GEOMETRY.

F. P.	ENERGY (KEV)	PEAK CHNL	CPS	GAMMA/SEC	ERR (%)	BW	MU	FWHM (KEV)	PK #
???	74.06	104.71	493.50	2.273E+06	1.17	31	3	3.86	1
CE144	80.05	113.31	172.56	6.514E+05	2.35	31	3	2.49	2
PR233	84.97	120.38	223.26	7.435E+05	1.95	31	3	3.01	3
EU155									
PR233	94.57	134.18	113.44	3.183E+05	2.72	15	2	2.36	4
PR233	98.32	139.55	188.32	5.044E+05	1.94	15	2	2.51	5
TE125	111.12	157.94	105.09	2.551E+05	4.78	14	1	2.43	6
PR233									
EU154	122.91	174.88	19.410	6.121E+04	16.12	8	1	2.48	7
CE144	133.45	190.03	1054.9	3.154E+06	0.56	15	1	2.29	8
SB125	427.90	612.98	22.370	1.405E+05	12.48	10	1	2.40	9
CS134	475.52	681.38	12.371	8.699E+04	15.86	7	1	1.98	10
RU106	511.87	733.58	1068.8	8.125E+06	0.45	16	1	2.55	11
CS134	563.30	807.45	61.995	5.209E+05	3.39	20	2	2.59	12
CS134	569.32	816.09	117.90	1.001E+06	2.32	20	2	2.50	13
CS134	604.75	866.97	674.81	6.101E+06	0.66	38	3	2.45	14
RU106	616.26	883.50	23.554	2.171E+05	6.08	38	3	2.36	15
RU106	622.10	891.88	410.44	3.819E+06	0.81	38	3	2.47	16
CS137	661.82	948.93	490.16	4.856E+06	0.76	20	2	2.86	17
CE144	696.57	998.83	39.952	4.166E+05	4.21	10	1	2.40	18
ZR95	724.21	1038.52	66.485	7.206E+05	2.84	12	1	2.64	19
EU154									
???	745.46	1069.03	1.9862	2.215E+04	42.58	5	1	0.70	20
ZR95	756.82	1085.33	72.596	8.216E+05	2.14	27	2	2.60	21
EU154									
NB95	765.87	1098.34	292.23	3.346E+06	1.00	27	2	2.58	22
AG110M									
CS134	795.90	1141.45	467.74	5.560E+06	0.62	21	2	2.68	23
CS134	801.99	1150.20	52.501	6.287E+05	2.47	21	2	2.74	24
RU106	873.66	1253.10	15.138	1.960E+05	10.63	15	2	2.74	25
EU154									
AG110M	884.77	1269.05	9.4612	1.245E+05	9.47	7	1	2.30	26
AG110M	937.60	1344.91	3.7125	5.161E+04	16.93	5	1	1.09	27
RU106	1050.47	1506.95	35.980	5.566E+05	3.91	17	2	2.89	28
???	1112.58	1596.11	2.6875	4.386E+04	33.61	13	1	2.46	29
EU154	1128.18	1618.50	8.4300	1.393E+05	7.86	8	1	2.51	30
RU106									
EU154	1274.49	1828.52	9.4800	1.755E+05	5.95	9	1	2.79	31
CS134	1365.18	1958.69	10.570	2.087E+05	5.57	12	1	3.00	32
???	1399.52	2007.96	.64000	1.293E+04	42.84	6	1	1.16	33
???	1407.87	2019.95	2.9075	5.911E+04	11.95	7	1	1.28	34
CE144	1488.82	2136.12	2.5062	5.543E+04	10.55	5	1	1.51	35
CE144	2185.70	3135.95	6.6337	2.078E+05	4.38	11	1	3.33	36

11 -16 -1977 1547.17

HT-31, U-17, PARTICLE #3; 30 CM GEOMETRY.

F. P.	ENERGY (KEV)	PEAK CHNL	CPS	GAMMA/SEC	ERR (%)	BW	MU	FWHM (KEV)	PK #
???	74.10	104.76	428.10	1.947E+06	1.30	48	5	4.10	1
CE144	79.93	113.14	149.36	5.597E+05	2.60	48	5	2.48	2
PA233	85.03	120.46	194.72	6.405E+05	2.10	48	5	3.18	3
EU155									
PA233	94.52	134.10	138.37	3.620E+05	2.90	48	5	2.11	4
PA233	98.34	139.58	229.83	6.007E+05	1.91	48	5	2.62	5
TE125	111.13	157.95	58.627	1.407E+05	6.10	9	1	2.67	6
PA233									
CE144	133.51	190.11	941.21	2.783E+06	0.59	14	1	2.40	7
KR85	512.15	733.98	960.64	7.227E+06	0.52	19	1	2.57	8
RU106									
CS134	563.49	807.71	60.869	5.060E+05	3.53	20	2	2.68	9
CS134	569.63	816.53	100.31	8.434E+05	2.61	20	2	2.73	10
CS134	605.07	867.43	617.92	5.528E+06	0.63	16	1	2.70	11
SB125									
RU106	616.61	884.01	21.951	2.002E+05	6.89	19	2	2.37	12
RU106	622.41	892.33	364.48	3.356E+06	0.69	19	2	2.71	13
CS137	662.08	949.29	418.37	4.101E+06	0.78	16	1	2.72	14
CE144	696.95	999.37	35.320	3.645E+05	4.66	10	1	2.87	15
ZR95	724.54	1038.99	56.961	6.109E+05	3.04	11	1	2.75	16
EU154									
ZR95	757.05	1085.67	63.282	7.006E+05	2.44	27	2	2.74	17
EU154									
NB95	766.12	1098.69	256.15	2.902E+06	1.12	27	2	2.83	18
CS134	796.27	1141.99	415.34	4.885E+06	0.76	27	3	2.75	19
CS134	802.50	1150.93	47.261	5.601E+05	2.82	27	3	18.0	20
RU106	873.95	1253.52	13.897	1.787E+05	7.71	9	1	2.49	21
EU154									
AG110M	885.27	1269.77	7.0425	1.021E+05	11.13	7	1	2.26	22
AG110M	937.32	1344.50	5.0950	7.804E+04	19.16	10	1	2.93	23
RU106	1050.92	1507.59	30.655	4.692E+05	3.50	12	1	2.90	24
CS134	1168.66	1676.61	2.7907	4.729E+04	23.27	9	1	2.78	25
EU154	1275.02	1829.28	7.6600	1.403E+05	6.75	8	1	2.91	26
CS134	1365.83	1959.61	7.2050	1.400E+05	6.63	9	1	3.09	27
CE144	1489.50	2137.11	2.1575	4.575E+04	11.88	5	1	1.39	28
???	1562.93	2242.43	2.1662	4.809E+04	12.64	7	1	3.10	29
CE144	2186.66	3137.33	5.0625	1.569E+05	5.60	13	1	3.20	30

11 -16 -1977 1552.37
HT-31, U-17, PARTICLE #4; 30 CM GEOMETRY.

F. P.	ENERGY (KEV)	PEAK CHNL	CPS	GAMMA/SEC	ERR (%)	BW	MU	FWHM (KEV)	PK #
???	74.91	105.93	468.98	2.064E+06	1.34	57	6	5.64	1
CE144	79.88	113.07	166.81	6.241E+05	2.49	57	6	2.54	2
PA233	84.73	120.03	217.06	7.168E+05	2.05	57	6	2.65	3
EU155									
PA233	94.50	134.07	151.68	4.201E+05	2.68	57	6	2.47	4
PA233	98.57	139.91	244.99	6.453E+05	1.92	57	6	3.19	5
TE125	111.14	157.98	70.744	1.693E+05	4.32	43	3	2.75	6
PA233									
CE144	133.46	190.04	1045.1	3.082E+06	1.07	43	3	2.29	7
SB125	428.02	613.16	17.265	1.070E+05	18.03	12	2	2.32	8
RU106	511.96	733.72	1021.8	7.663E+06	0.44	15	1	2.57	9
CS134	563.33	807.48	62.855	5.143E+05	3.39	20	2	2.66	10
CS134	569.55	816.42	110.83	9.291E+05	2.38	20	2	2.66	11
CS134	604.96	867.27	663.12	5.915E+06	0.60	17	1	2.66	12
SB125									
RU106	616.40	883.70	26.791	2.436E+05	5.51	21	2	2.97	13
RU106	622.19	892.01	408.33	3.748E+06	0.83	21	2	2.58	14
CS137	661.86	948.99	447.44	4.372E+06	0.70	15	1	2.61	15
CE144	696.65	998.94	38.400	3.950E+05	4.23	10	1	2.39	16
ZR95	724.29	1038.62	67.730	7.041E+05	2.67	12	1	2.95	17
EU154									
ZR95	756.94	1085.51	69.784	7.791E+05	2.18	25	2	2.72	18
EU154									
NB95	766.82	1098.54	279.50	3.157E+06	0.97	25	2	2.76	19
CS134	796.82	1141.63	455.77	5.344E+06	0.65	24	2	2.80	20
CS134	801.93	1150.11	50.993	6.022E+05	2.53	24	2	3.24	21
RU106	873.55	1252.94	14.600	1.872E+05	6.74	8	1	2.42	22
EU154									
???	964.28	1383.21	2.3800	3.351E+04	29.17	7	1	2.09	23
RU106	1050.78	1507.40	36.227	5.528E+05	2.83	11	1	2.88	24
EU154	1128.54	1619.02	8.0900	1.319E+05	7.87	8	1	2.72	25
RU106									
CS134	1167.64	1675.14	2.5025	4.213E+04	19.44	6	1	1.63	26
EU154	1274.80	1828.96	9.9350	1.815E+05	6.45	12	1	3.17	27
CS134	1365.56	1959.23	9.5350	1.858E+05	5.29	10	1	2.96	28
CE144	1489.51	2137.12	2.8400	6.006E+04	10.11	6	1	2.45	29
???	1562.53	2241.91	2.8900	6.396E+04	9.85	8	1	3.55	30
???	1948.66	2795.92	.27000	7.418E+03	39.95	5	1	1.76	31
CE144	2186.12	3136.54	6.9525	2.148E+05	4.39	14	1	3.15	32

11 -16 -1977 1602.25

HT-31, U-17, PARTICLE #5; 30 CM GEOMETRY.

F. P.	ENERGY (KEV)	PEAK CHNL	CPS	GAMMA/SEC	ERR (%)	BW	MU	FWHM (KEV)	PK #
???	74.26	104.98	444.08	2.010E+06	1.68	80	9	3.86	1
CE144	80.10	113.39	151.01	5.636E+05	2.95	80	9	2.45	2
PA233	85.82	120.45	204.49	6.735E+05	2.40	80	9	3.08	3
EU155									
PA233	94.83	134.54	150.31	4.161E+05	2.87	80	9	2.78	4
PA233	98.33	139.57	253.19	6.713E+05	2.11	80	9	2.59	5
TE125	111.16	158.61	94.969	2.282E+05	4.01	80	9	2.98	6
PA233									
CE144	133.49	190.09	991.89	2.936E+06	0.56	14	1	2.32	7
SB125	427.96	613.07	23.823	1.482E+05	10.62	9	1	2.82	8
RU103	497.77	713.33	6.9625	5.088E+04	20.60	5	1	1.38	9
RU106	511.96	733.71	1026.4	7.728E+06	0.46	17	1	2.52	10
CS134	563.39	807.57	60.239	5.012E+05	3.45	20	2	2.78	11
CS134	569.54	816.40	113.03	9.512E+05	2.36	20	2	2.73	12
CS134	604.84	867.10	668.30	5.983E+06	0.58	16	1	2.55	13
SB125									
RU106	616.36	883.64	27.446	2.505E+05	5.35	20	2	2.34	14
RU106	622.19	892.02	399.36	3.680E+06	0.83	20	2	2.61	15
AG110M	657.80	943.15	20.347	1.984E+05	6.19	17	2	1.93	16
CS137	661.85	948.97	439.34	4.310E+06	0.67	17	2	2.54	17
CE144	696.67	998.97	36.005	3.718E+05	4.21	9	1	2.40	18
ZR95	724.25	1038.57	62.050	6.659E+05	3.91	18	2	2.75	19
EU154									
ZR95	756.89	1085.44	70.322	7.881E+05	2.20	26	2	2.65	20
EU154									
NB95	765.98	1098.49	275.39	3.122E+06	1.01	26	2	2.80	21
AG110M									
CS134	796.02	1141.63	455.83	5.366E+06	0.64	22	2	2.70	22
CS134	801.88	1150.04	47.239	5.600E+05	2.68	22	2	3.19	23
RU106	873.64	1253.08	15.356	1.976E+05	7.00	9	1	2.98	24
EU154									
AG110M	885.01	1269.40	10.313	1.344E+05	8.47	7	1	2.62	25
AG110M	937.15	1344.26	3.0525	4.208E+04	19.62	5	1	1.84	26
RU106	1050.73	1507.31	35.255	5.401E+05	2.93	11	1	2.88	27
???	1112.72	1596.31	1.2987	2.099E+04	42.65	7	2	1.13	28
EU154	1128.18	1618.51	7.1350	1.168E+05	10.49	10	1	2.61	29
RU106									
CS134	1168.24	1676.00	4.0612	6.868E+04	16.23	9	1	2.95	30
EU154	1274.57	1828.63	10.002	1.834E+05	5.55	9	1	3.20	31
???	1333.35	1913.00	2.8550	5.461E+04	12.89	7	1	3.64	32
CS134	1365.67	1959.38	9.6687	1.891E+05	5.55	11	1	3.09	33
AG110M	1384.39	1986.26	1.6137	3.197E+04	16.85	5	1	1.40	34
???	1408.07	2020.23	4.1162	8.287E+04	9.56	9	1	3.77	35
CE144	1489.45	2137.03	2.5475	5.408E+04	10.53	5	1	2.16	36
CE144	2186.34	3136.86	7.0375	2.183E+05	4.73	22	2	3.49	37